

# Chromosome-level assembly and analysis of the *Thymus* genome provide insights into glandular secretory trichome formation and monoterpenoid biosynthesis in thyme

Meiyu Sun<sup>1,4</sup>, Yanan Zhang<sup>1,2,4</sup>, Li Zhu<sup>1,2</sup>, Ningning Liu<sup>1,2</sup>, Hongtong Bai<sup>1</sup>, Guofeng Sun<sup>3</sup>, Jinzheng Zhang<sup>1,\*</sup> and Lei Shi<sup>1,\*</sup>

<sup>1</sup>Key Laboratory of Plant Resources and Beijing Botanical Garden, Institute of Botany, Chinese Academy of Sciences, Beijing 100093, China

<sup>2</sup>University of Chinese Academy of Sciences, Beijing 100049, China

<sup>3</sup>Beijing Botanical Garden, Institute of Botany, Chinese Academy of Sciences, Beijing 100093, China

<sup>4</sup>These authors contributed equally to this article.

\*Correspondence: Jinzheng Zhang (caohua@ibcas.ac.cn), Lei Shi (shilei\_67@126.com)

<https://doi.org/10.1016/j.xplc.2022.100413>

## ABSTRACT

Thyme has medicinal and aromatic value because of its potent antimicrobial and antioxidant properties. However, the absence of a fully sequenced thyme genome limits functional genomic studies of Chinese native thymes. *Thymus quinquecostatus* Čelak., which contains large amounts of bioactive monoterpenes such as thymol and carvacrol, is an important wild medicinal and aromatic plant in China. Monoterpenoids are abundant in glandular secretory trichomes. Here, high-fidelity and chromatin conformation capture technologies were used to assemble and annotate the *T. quinquecostatus* genome at the chromosome level. The 13 chromosomes of *T. quinquecostatus* had a total length of 528.66 Mb, a contig N50 of 8.06 Mb, and a BUSCO score of 97.34%. We found that *T. quinquecostatus* had experienced two whole-genome duplications, with the most recent event occurring ~4.34 million years ago. Deep analyses of the genome, in conjunction with comparative genomic, phylogenetic, transcriptomic, and metabonomic studies, uncovered many regulatory factors and genes related to monoterpenoids and glandular secretory trichome development. Genes encoding terpene synthase (TPS), cytochrome P450 monooxygenases (CYPs), short-chain dehydrogenase/reductase (SDR), R2R3-MYB, and homeodomain-leucine zipper (HD-ZIP) IV were among those present in the *T. quinquecostatus* genome. Notably, *Tq02G002290.1* (*TqTPS1*) was shown to encode the terpene synthase responsible for catalyzing production of the main monoterpane product  $\gamma$ -terpinene from geranyl diphosphate (GPP). Our study provides significant insight into the mechanisms of glandular secretory trichome formation and monoterpenoid biosynthesis in thyme. This work will facilitate the development of molecular breeding tools to enhance the production of bioactive secondary metabolites in Lamiaceae.

**Key words:** *Thymus quinquecostatus*, chromosome-level genome, phylogenetics, glandular secretory trichome, monoterpenoids

**Sun M., Zhang Y., Zhu L., Liu N., Bai H., Sun G., Zhang J., and Shi L.** (2022). Chromosome-level assembly and analysis of the *Thymus* genome provide insights into glandular secretory trichome formation and monoterpenoid biosynthesis in thyme. *Plant Comm.* **3**, 100413.

## INTRODUCTION

The genus *Thymus*, which belongs to the Lamiaceae family, is widely distributed worldwide and predominantly found in the Mediterranean basin. *Thymus* contains more than 300 species of herbaceous perennials or subshrubs with valuable medicinal and aromatic properties (Stahl-Biskup and Venskutonis, 2012).

The Chinese native thyme species *Thymus quinquecostatus* Čelak. is widely used in folk medicine for the treatment of

---

Published by the Plant Communications Shanghai Editorial Office in association with Cell Press, an imprint of Elsevier Inc., on behalf of CSPB and CEMPS, CAS.

## Plant Communications

stroke, cold, dyspepsia, toothache, acute gastroenteritis, hypertension, chronic eczema, and other diseases (Kim et al., 2015a). Furthermore, it is used alone or in combination with other herbal medicines in cancer treatment (Hong et al., 2020). In China, *T. quinquecostatus* is also called *di jiao* (地椒). In some parts of China, *di jiao* is used not only in folk medicine but also as a seasoning or as fodder for livestock to improve the taste of their meat. One example in which *T. quinquecostatus* is used for livestock fodder is with the “*di jiao* sheep” in the Loess Plateau region. In addition to its medicinal and edible value, *T. quinquecostatus* has an important ecological function in changing soil microbiological properties during grass litter decomposition (Xiang et al., 2018) because it has relatively short stolons, which can form very strong root networks to prevent soil erosion.

The antibacterial and antioxidant medicinal functions of *T. quinquecostatus* depend on the bioactive components thymol, carvacrol, citral, geraniol, and nerolidol (Kou et al., 2008; Gavarić et al., 2015; Chan et al., 2016; Tak and Isman, 2016; Benelli et al., 2017; Pavela et al., 2018). The vast majority of these compounds are terpenoids. The evolution of terpenoid biosynthesis can be better understood by investigating terpene synthases (TPSs). Plant terpenoids contain isopentenyl diphosphate (C-5) and isomeric dimethylallyl diphosphate building blocks that are derived from the cytosolic mevalonate (MVA) or plastidial methylerythritol phosphate (MEP) pathways (Tholl, 2006; Dudareva and Pichersky, 2008; Zhou and Pichersky, 2020). TPS catalyzes the formation of the basic monoterpene (C10) and sesquiterpene (C15) skeletons from geranyl diphosphate (GPP) and farnesyl diphosphate (FPP), respectively. In previous studies of thyme, thymol and carvacrol biosynthesis was proposed to cyclize GPP to  $\gamma$ -terpinene, followed by a series of oxidations via *p*-cymene (Lima et al., 2013). The expression of  $\gamma$ -terpinene synthase genes was found to be related to thymol and carvacrol content. Examples of  $\gamma$ -terpinene synthase genes are *OvTPS2* in *Origanum vulgare* (oregano) (Crocoll et al., 2010), *TvTPS2* in *Thymus vulgaris* (Behnaz et al., 2020), and *TcTPS2* in *Thymus caespititius* (Lima et al., 2013). Furthermore, a new study has shown that the aromatic backbones of thymol and carvacrol are formed by the CYP71D subfamily and short-chain dehydrogenase/reductase (SDR) in combination with dehydrogenases via unstable intermediates (Krause et al., 2021). Although TPSs that form  $\gamma$ -terpinene have been identified and characterized in various European thyme species, there are no reports on phenolic monoterpene precursors and terpene biosynthetic pathways in Chinese native thyme.

Plant secondary metabolites, such as terpenoids, are synthesized and stored in trichomes, which are hair-like extensions of leaf, flower, and stem epidermal cells. Depending on the plant species, trichomes consist of a single cell or multiple cells and are classified as either glandular or nonglandular trichomes (Werker, 2000). Mint, basil, lavender, oregano, and thyme (Lamiaceae) are cultivated for the terpenoids produced in their glandular secretory trichomes (Maleci and Giuliani, 2006). Glandular secretory trichome density was shown to be positively correlated with the production of terpenes (Yan et al., 2017). Consequently, increasing the density of glandular secretory trichomes could be an effective approach for improving the production of these natural metabolites (Tissier,

## Chromosome-level genome of *Thymus quinquecostatus*

2012). Knowledge about genes involved in glandular secretory trichome formation comes mostly from work on *Artemisia annua*, *Nicotiana benthamiana* (tobacco), and *Solanum lycopersicum* (tomato) (Robert and Tissier, 2020). Through these studies, transcription factors (R2R3-MYB and HD-ZIP IV), cell cycle regulators (CycB2), and receptors involved in phytohormone-induced signaling cascades were implicated in glandular secretory trichome development. However, nothing is known about the molecular mechanism underlying glandular secretory trichome formation in Lamiaceae species. Uncovering genetic networks that control glandular secretory trichome formation in Lamiaceae will not only enable in-depth studies of plant secondary metabolism but also guide breeding strategies to improve terpene production (Huchelmann et al., 2017; Chalvin et al., 2020).

Here we report a reference genome sequence of *T. quinquecostatus*, which was obtained using a combination of high-fidelity (HiFi) sequencing and chromatin conformation capture (Hi-C) technologies. Genome-scale analyses of the sequencing data along with comparative genomic, phylogenetic, transcriptomic, and metabolomic studies revealed mechanisms that underlie glandular secretory trichome formation and monoterpenoid biosynthesis in *T. quinquecostatus*. The *T. quinquecostatus* genome presented here provides a resource that will also facilitate research on molecular breeding and functional gene identification related to important characteristics in thyme.

## RESULTS AND DISCUSSION

### Sequencing, assembly, and annotation of the *T. quinquecostatus* genome

Plants in the Lamiaceae family are distributed worldwide. Some members of this family, such as thyme, lavender, mint, basil, rosemary, marjoram, perilla, sage, and skullcap, are medicinal plants that contain a diverse set of specialized metabolites (Wu, 1977). Terpenoids, phenolic acids, and flavonoids are the most common plant secondary metabolites in Lamiaceae (Wu et al., 2016; Zhao et al., 2016). A high-quality genome sequence would provide a key resource for advancing studies on the molecular basis of specialized metabolite diversity in different members of Lamiaceae and would promote a better understanding of the evolution of pathways involved in the biosynthesis of plant secondary compounds (Afendi et al., 2012).

We sequenced the genome of *T. quinquecostatus* using Illumina HiSeq and PacBio technologies (Supplemental Tables 1–3). We obtained 21.74 Gb of PacBio circular consensus sequencing (CCS) reads (Cheng et al., 2021), amounting to 39.80 $\times$  coverage of the ~546.18 Mb genome, whose size was estimated by k-mer distribution analysis (Supplemental Figure 1; Table 1). We measured the genome size to be 536.25 Mb using flow cytometry, which was close to the value given by the k-mer method (Supplemental Figure 1). Finally, a chromosome-level genome was obtained, which contained 13 pseudochromosomes with a total length of 528.66 Mb (Figure 2; Supplemental Figure 2; Table 1), a contig N50 of 8.06 Mb, and a scaffold N50 of 36.44 Mb (Table 1).

The accuracy and completeness of the assembled *T. quinquecostatus* genome were validated using short-read



**Figure 1. Overview of the morphological characteristics of *T. quinquecostatus*.**

- (A) Plant at the flowering stage.
- (B) Root.
- (C) Stem.
- (D) Leaf.
- (E) Flower at the bud stage.
- (F) Flower at the half-open stage.
- (G) Flower at the full-open stage.

sequence alignment, Benchmarking Universal Single-Copy Orthologs (BUSCO), and Core Eukaryotic Genes Mapping Approach (CEGMA). Illumina short reads were mapped to the assembly and showed a mapping rate of 95.26% for the short reads and a mapping coverage of 89.47% for the assembled genome. Furthermore, 91.41% (exon), 6.57% (intergenic), and 2.03% (intron) of the sequences from these transcripts were successfully aligned. BUSCO analysis showed that 97.34% of the conserved genes belonged to complete and single-copy, com-

plete and duplicated, fragmented, and missing categories, which accounted for 1499 (92.87%), 72 (4.46%), 16 (0.99%), and 27 (1.67%) of the total genes, respectively. CEGMA showed that 97.82% of the assembled *T. quinquecostatus* genome was reliably annotated (Table 1).

A Hi-C heatmap showed that interactions within chromosomes were more frequent than those between chromosomes, which suggested that the Hi-C assembly (Servant et al., 2015) was of

Parameter	Size or number
Estimate of genome size (flow cytometry), Mb	536.25
Estimate of genome size (survey), Mb	546.18
Assembled genome size, Mb	528.66
Total length of contigs, Mb	528.66
Total number of contigs	628
N50 of contigs, bp	8,059,748
Largest contig, bp	17,334,620
Total length of scaffolds, Mb	528.68
Total number of scaffolds	478
N50 of scaffolds, bp	36,440,660
Largest scaffold, bp	49,018,360
GC content, %	40.40
Complete CEGMA, %	97.82
Complete BUSCOs, %	97.34
Total length of repeat, Mb	373.28
Repeat density, %	70.61
Long terminal repeat (LTR) density, %	61.47
Microsatellite repeat density, %	9.14
Number of protein-coding genes	29,676
Number of annotated genes	28,862
Number of rRNA	2557
Number of tRNA	1138
Number of miRNAs	58
Number of snRNAs	86
Number of snoRNAs	68
Number of pseudogenes	217

**Table 1.** Global statistics of *T. quinquecostatus* genome assembly and annotation

high quality (Supplemental Figure 2). A total of 478 scaffolds were constructed, and the longest scaffold was 49.02 Mb (Supplemental Tables 4–6). A total of 506.90 Mb of sequences were anchored onto 13 pseudochromosomes, accounting for 95.88% of the initial assembly (Supplemental Table 6). In addition, Hi-C data mapped against the Hi-C scaffold assembly showed 488.75 Mb of sequences for determining the order and direction in 13 pseudochromosomes and a 96.42% valid rate of assembled sequences (Supplemental Table 6). Taken together, these statistics verified that our genome assembly is precise, complete, and of high quality at the chromosome scale.

The *T. quinquecostatus* genome was highly repetitive, with a total of 373.28 Mb of repetitive sequences annotated, accounting for 70.61% of the genome (Table 1). Long terminal repeat (LTR) retrotransposons were the dominant repeat type, taking up 324.98 Mb (61.47%) of the genome (Figure 2; Supplemental Table 7). LTRs consisted of two major types, class I (retroelement) and class II (DNA transposon), which represented 54.41% and 7.06% of the assembled genome, respectively. In addition, 239400 tandem repeats were

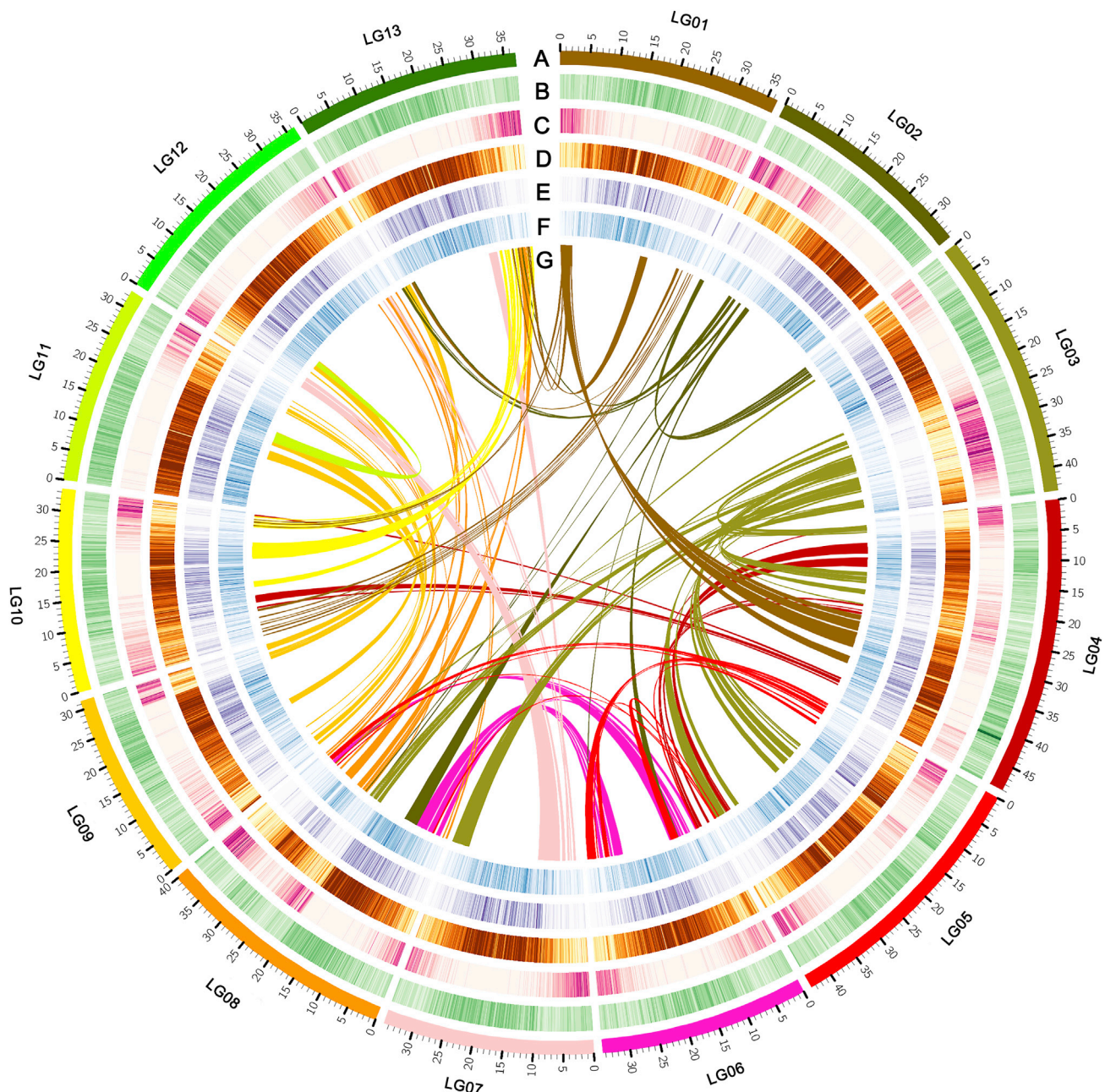
identified, accounting for 48.30 Mb (9.14%) of the genome (Supplemental Table 8).

A total of 29676 protein-coding genes were predicted, with 28862 (97.26%) annotated by incorporating transcriptome, homology, and *ab initio* prediction (Supplemental Tables 9–11; Supplemental Figure 3) (Haas et al., 2008). Statistical gene information for *T. quinquecostatus* and the other species, including *Arabidopsis thaliana*, *Ocimum tenuiflorum*, *Scutellaria baicalensis*, *Salvia miltiorrhiza*, *Salvia splendens*, and *Tectona grandis*, showed an average *T. quinquecostatus* gene length of 3155.30 bp, a coding sequence length of 1315.72 bp, and an exon number of 5.25 (Supplemental Figure 3; Supplemental Table 10). Functional annotation of these genes against the published databases Pfam, Swiss-Prot, TrEMBL, EggNOG (Supplemental Figure 4A), and nr (Supplemental Table 11) resulted in 85.38%, 79.14%, 96.66%, 83.74%, and 96.71% functionally assigned genes, respectively. We further annotated these genes using the EuKaryotic Orthologous Groups (KOG), Gene Ontology (GO) (Supplemental Figure 4B), and Kyoto Encyclopedia of Genes and Genomes (KEGG) databases (Supplemental Table 11). We also identified 58 micro-RNAs (miRNAs), 86 small nuclear RNAs (snRNAs), 68 small nucleolar RNAs (snoRNAs), 1138 tRNAs, 2557 rRNAs, and 217 pseudogenes in the *T. quinquecostatus* genome (Table 1).

#### Evolutionary and comparative genomic analyses of *T. quinquecostatus*

To investigate the evolutionary history of *T. quinquecostatus*, we analyzed the genomes of 15 selected angiosperm species: *A. thaliana*, *A. annua*, *Cucumis sativus*, *Medicago truncatula*, *Nicotiana tabacum*, *O. tenuiflorum*, *Panicum virgatum*, *S. miltiorrhiza*, *S. splendens*, *S. baicalensis*, *Sesamum indicum*, *S. lycopersicum*, *Sorghum bicolor*, *T. grandis*, and *Vitis vinifera* (Supplemental Table 12). Maximum likelihood-based phylogenetic analyses were performed with *V. vinifera* as the outgroup. The most recent common ancestor (MRCA) of the 16 species contained 44276 gene families and 951 high-quality single-copy orthologous genes (Figure 3A). The results indicated that *T. quinquecostatus* is closely related to *O. tenuiflorum*, *S. splendens*, and *S. miltiorrhiza* (Figure 3A). Molecular dating using *V. vinifera* for fossil calibration indicated that *T. quinquecostatus*-*O. tenuiflorum* emerged ~29.51 (19.72–40.24) million years ago (Mya) and that *T. quinquecostatus*-two *Salvia* species (*S. splendens* and *S. miltiorrhiza*) emerged ~22.77 (14.80–31.50) Mya.

A total of 65100 gene families were identified in the 16 selected angiosperm species, and 1873 common gene families with 479 unique gene families were uncovered in the *T. quinquecostatus* genome (Supplemental Figure 5A; Supplemental Table 13). We compared the gene families among five Lamiaceae species. As shown in Supplemental Figure 5B, 7017 gene families were shared among *O. tenuiflorum*, *T. quinquecostatus*, *S. miltiorrhiza*, *T. grandis*, and *S. splendens*, and 1127 gene families were specific to *T. quinquecostatus*. There were 2442 expanded gene families and 8 contracted gene families (Supplemental Figures 7 and 8), suggesting that more *T. quinquecostatus* gene families experienced expansion than contraction during adaptive evolution. KEGG enrichment analysis showed that most of the rapidly expanded gene families clustered in

**Figure 2. Circos plot showing *T. quinquecostatus* genomic features.**

- (A) Karyotyping results.
- (B) GC content.
- (C) Protein-coding gene density.
- (D) DNA transposable element density.
- (E) LTR/Copia transposable element density.
- (F) LTR/Gypsy transposable element density.
- (G) Schematic presentation of major interchromosomal relationships in the *T. quinquecostatus* genome. The chromosome size is shown in Mb.

the flavonoid, photosynthetic, anthocyanin, phenylpropanoid, flavone, flavonol biosynthetic, and phenylalanine metabolism pathways ([Supplemental Figure 7E](#)), whereas contracted gene families clustered in the sesquiterpenoid and triterpenoid, monoterpenoid, cutin, suberin, and wax biosynthetic pathways ([Supplemental Figure 8E](#)). These metabolic processes may be related to *T. quinquecostatus* flower color, as well as terpenoid

and lignin biosynthesis. Functional annotation of expanded and contracted gene families accounted for various traits of *T. quinquecostatus*, including flower color and high terpene levels. The expansion and contraction of gene families may have played an essential role in the evolution of *T. quinquecostatus*, contributing to phenotypic diversification, environmental adaptation, and even speciation.

## Plant Communications

There are many common events in eudicots, including ancient polyploidizations, that act as an important evolutionary force driving speciation (Wood et al., 2009). To evaluate the evolutionary relationships among *T. quinquecostatus* and other plant species, we measured the synonymous substitution rates (Ks) of orthologous gene pairs. The distribution of these rates suggested that *T. quinquecostatus* experienced two whole-genome duplication (WGD) events in its evolutionary history (Zwaenepoel and Van de Peer, 2019). Two WGD events were investigated in the *T. quinquecostatus* genome on the basis of the distribution of Ks values of ~0.07 and ~1.22 between orthologs, corresponding to divergence at ~4.34 and ~70.97 Mya, respectively. The analysis revealed peaks of ~0.39 for *T. quinquecostatus*-*S. miltiorrhiza* and ~0.68 for *T. quinquecostatus*-*S. baicalensis*, corresponding to divergence at ~22.77 and ~44.73 Mya, respectively (Figure 3B). Analysis of the distribution of sequence divergence (4DTv) values for syntenic duplicate genes revealed two significant peaks for the *T. quinquecostatus* genome (4DTv ~0.02 and ~0.41; Figure 3C), which further confirmed that *T. quinquecostatus* had experienced two WGD events. A divergence peak value (4DTv ~0.15 and ~0.26) was observed for *T. quinquecostatus*-*S. miltiorrhiza* and *T. quinquecostatus*-*S. baicalensis* in the map (Figure 3C), which suggested that the divergence of *T. quinquecostatus*-*S. miltiorrhiza* occurred later than that of *T. quinquecostatus*-*S. baicalensis*. During the evolution of plant genomes, the frequency of WGD and polyploidization was high, resulting in a large proportion of duplicated genes and repetitive sequences (Lockton and Gaut, 2005). We found that *T. quinquecostatus*, like many other flowering plants, experienced two rounds of WGD, with the recent event occurring ~4.34 Mya, followed by extensive genomic rearrangements that resulted in 13 chromosomes in thyme after its divergence from the common paleopolyploid ancestor (Wei et al., 2018; Xia et al., 2020).

Accumulation of LTR-retrotransposons (LTR-RTs) is an important contributor to genome expansion and diversity (Kidwell and Lisch, 1997). A comparison of the insertion ages for LTR-RTs showed similar insertion profiles among the genomes. We found that most LTR-RT insertion events in the *T. quinquecostatus* genome occurred recently or less than 1 Mya. Nevertheless, the *T. quinquecostatus* genome contains fewer ancient insertions (>1 Mya) and more recent LTR-RT insertions (<1 Mya) than that of *N. tabacum* (Figure 3D). We also observed that the genomes of *P. virgatum*, *S. baicalensis*, and *T. quinquecostatus* carried younger LTR-RTs; the highest proportion of LTR-retrotransposons had insertion times of ~0.23, 0.32, and 0.33 Mya, respectively. This may have resulted from rapid changes in the environment, such as the effects of pathogens and interference from human activities, that have occurred in recent years. Overall, these findings provide new insights into the evolution of *T. quinquecostatus*.

To analyze colinear relationships within the *T. quinquecostatus*, *S. baicalensis*, and *V. vinifera* genomes, we identified homologous proteins using BLASTP and syntenic blocks using MCScanX. A total of 935 and 520 syntenic blocks were identified on the basis of the orthologous gene orders between *T. quinquecostatus*-*S. baicalensis* and *T. quinquecostatus*-*V. vinifera*, corresponding to 19740 and 9577 gene pairs in *T. quinquecostatus*-*S. baicalensis* and *T. quinquecostatus*-*V. vinifera*, respectively.

## Chromosome-level genome of *Thymus quinquecostatus*

(Supplemental Figures 9–11). A total of 282 syntenic blocks and 3263 gene pairs were identified in intragenomic comparisons of *T. quinquecostatus*-*T. quinquecostatus* (Supplemental Figure 11). The frequency of large-scale fragment rearrangements was determined in the three genomes, including inversions and translocations. The dot and bar graphs showed that *T. quinquecostatus*-*S. baicalensis* had higher collinearity than *T. quinquecostatus*-*V. vinifera*, consistent with their close phylogenetic relationship as members of the Lamiaceae clade (Supplemental Figures 9 and 10).

To date, there are only a few reports on the genomes of *S. miltiorrhiza*, *S. splendens*, *S. baicalensis*, and *Lavandula angustifolia* from Lamiaceae (Xu et al., 2016a; Dong et al., 2018; Zhao et al., 2019; Li et al., 2021). We now provide a high-quality reference genome sequence for *T. quinquecostatus*, which is the first genome for the genus *Thymus*. This genomic information provides a foundation for comparative genomic analysis between members of Lamiaceae.

### Transcriptome sequencing and phylogenetic analysis reveal the genetic mechanism of glandular secretory trichome formation

To identify genes that play important roles in glandular secretory trichome formation and monoterpenoid biosynthesis, we performed transcriptomic analyses of *T. quinquecostatus* and *T. vulgaris* ‘Elisbeth.’ A total of 33 complementary DNA (cDNA) libraries were processed for transcriptome sequencing, generating 238.49 Gb of clean data (Supplemental Figure 12). After data filtering, the Q30 values were greater than 93.68%. For individual samples, clean reads varied from 5.98 to 9.31 Gb (Supplemental Table 14). The comparison rate of all reads was ≥44.13%, and the unique mapping rate was ≥43.10% (Supplemental Table 15).

Glandular secretory trichomes can synthesize, store, or secrete monoterpenoids (Maleci and Giuliani, 2006; Yan et al., 2017). The type, size, and density of glandular secretory trichomes are shown in Figures 4A–4C. Glandular secretory trichomes were located mainly in leaves and flowers, and there were a few glandular secretory trichomes on the stems. The quantities of glandular secretory trichomes on leaves in *T. vulgaris* ‘Elisbeth’ (13 per mm<sup>2</sup>) were significantly higher than those in *T. quinquecostatus* (5 per mm<sup>2</sup>) (Figures 4A and 4B). Thyme contains two types of glandular secretory trichomes: capitate glandular trichomes and peltate glandular trichomes (Figure 4C). By searching and collecting information on regulatory genes related to glandular secretory trichome formation in *A. annua*, *N. benthamiana*, and *S. lycopersicum*, we summarized the genetic network of glandular secretory trichome formation in thyme (Figure 4C). The formation of glandular secretory trichomes has four stages: determination, initiation, morphogenesis, and maturation. Given their common organizational scheme, it has been suggested that glandular secretory trichomes share similar developmental events among different plant species (Chalvin et al., 2020). The initiation of most glandular secretory trichomes is regulated by MYB and HD-ZIP transcription factors (TFs). In *A. annua*, *AaMYB1* positively regulates the development of glandular secretory trichomes (Matías-Hernández et al., 2017). *AaMIXTA1* interacts with *AaHD8*

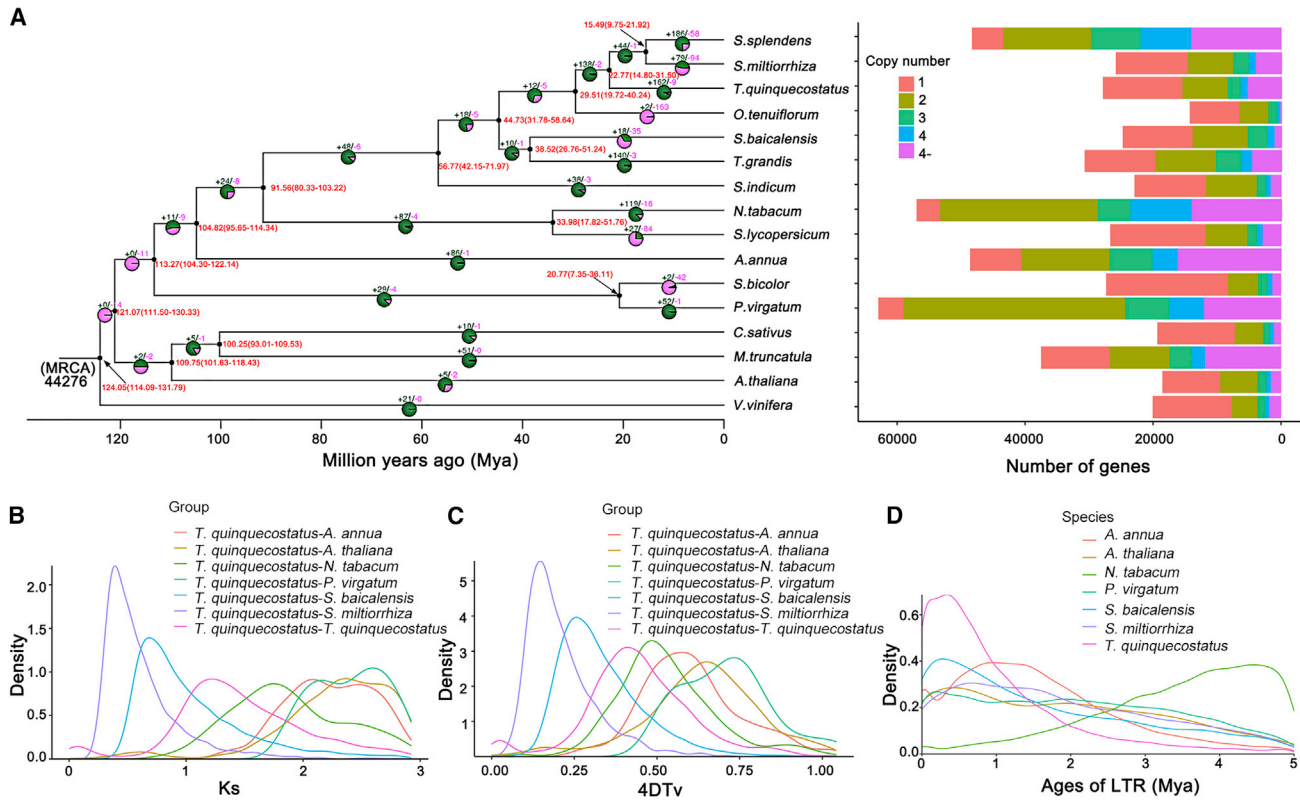


**Figure 3. Genome comparison and evolutionary analysis.**

**(A)** Phylogenetic analysis, divergence time estimates, and the number of gene copies and their distribution among 16 plant species. The tree was constructed on the basis of 951 single-copy truly orthologous genes. Divergence times (Mya) are indicated by the red numbers beside the branch nodes. The numbers of gene-family expansion and contraction events are indicated by green and pink numbers, respectively, on each species branch. MRCA, most recent common ancestor.

**(B)** Distribution of the synonymous substitution rate ( $K_s$ ) between *T. quinquecostatus* and *A. annua*, *A. thaliana*, *N. tabacum*, *P. virgatum*, *S. baicalensis*, *S. miltiorrhiza*, and *T. quinquecostatus*.

**(C)** Genome duplication in *T. quinquecostatus* and genomes of related species as revealed by 4DTv analyses.

**(D)** Distribution of insertion ages of LTR-retrotransposons in the genomes of *T. quinquecostatus* and genomes of related species. LTR, long terminal repeat; Mya, million years ago.

to form a regulatory complex that directly promotes *AaHD1* expression and positively regulates the initiation of glandular secretory trichomes (Yan et al., 2017, 2018; Shi et al., 2018). *AaTRICHOME AND ARTEMISININ REGULATOR* (*AaTAR2*) can also positively modulate glandular secretory trichomes, and *AaHD1* and *AaHD8* enhance the expression of *AaTAR2* by directly binding to its promoter (Zhou et al., 2020). In tomato, formation of type I capitate glandular trichomes involves the *Woolly* gene, which encodes an HD-ZIP TF, together with *SiCyCB2*. In addition, the *Hair* gene, which encodes a C2H2 zinc finger protein, can interact with *Woolly* (Chang et al., 2018). In tobacco, *NbMYB123-like* (homolog of *AtMYB123*), which encodes a putative R2R3-MYB domain TF, also participates in the development of glandular secretory trichomes (Liu et al., 2018). In addition to TFs, glandular secretory trichome initiation is known to be regulated by plant hormones (Maes and Goossens, 2010) such as jasmonates (JA) (Yan et al., 2017), indole-3-acetic acid (IAA) (Zhang et al., 2015), and gibberellic acid (GA) (Chen et al., 2020).

We summarized the genetic network that modulates glandular secretory trichome formation in thyme based on identified TFs

(Figure 4C). We found that two TFs, including R2R3-MYB (encoded by *MYB1*, *MIXTA1*, *TAR2*, and *MYB123-like*) and HD-ZIP IV (encoded by *HD8*, *HD1*, and *Woolly*), are involved in thyme glandular secretory trichome development. Sequence similarity search results showed that 175 MYB-encoding and 87 HD-ZIP-encoding genes were identified in the *T. quinquecostatus* genome. In addition to hormone-related genes (*IAA15*, *JAZ2*, *JAZ8*, and *ARF3*), genes such as *Glandular trichome-Specific WRKY 2* (*GSW2*), *MYC1*, *B-type cyclin 2* (*CyCB2*), *Glabrous Inflorescence Stems* (*G1S*), *Transparent Testa Glabra 1* (*TTG1*), and *Hair* were involved in glandular secretory trichome formation. A heatmap showed that 142 MYB-encoding (Supplemental Figure 13A) and 68 HD-ZIP-encoding DEGs (Figure 4D) were involved in glandular secretory trichome formation (Figure 4C). We also identified 62 hormone-related genes (29 *IAA15*s, 4 *JAZ2*s, 5 *JAZ8*s, and 24 *ARF3*s), 63 *GSW2*s, 62 *MYC1*s, 26 *CyCB2*s, 15 *G1S*s, 11 *TTG1*s, and three *Hairs* that were differentially expressed in thyme (Supplemental Figure 13).

Phylogenetic tree analysis (Kumar et al., 2018) of MYB- and HD-ZIP-encoding DEGs in *T. quinquecostatus* and other species

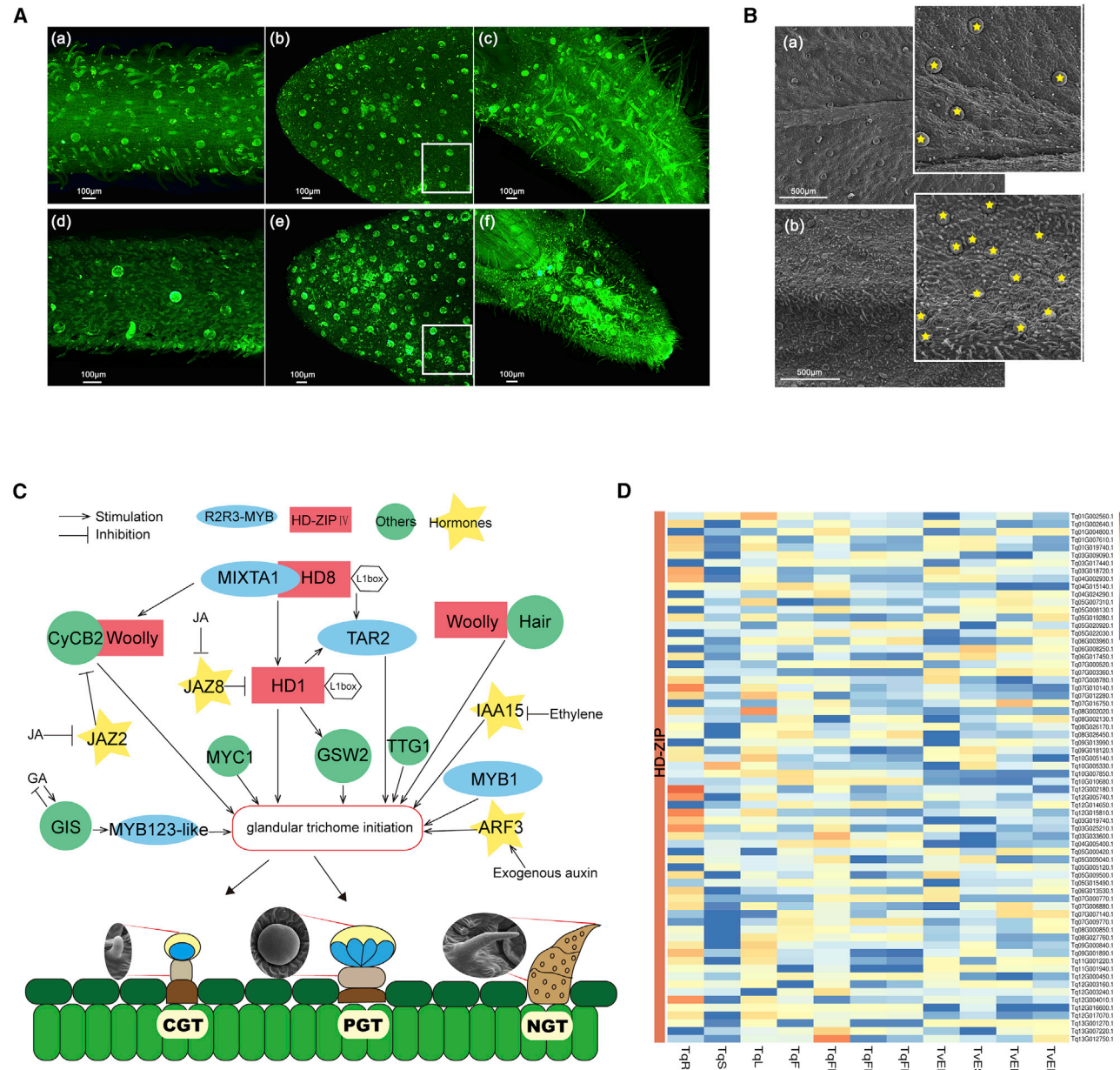


**Figure 4. Schematic overview of glandular secretory trichome formation in thyme.**

**(A)** The density of glandular secretory trichomes is shown in *T. quinquecostatus* and *T. vulgaris* 'Elstbeth' by fluorescence microscopy. (a) TqStem. (b) TqLeaf. (c) TqFlower. (d) TvEStem. (e) TvELeaf. (f) TvEFlower. Tq, *T. quinquecostatus*; TvE, *T. vulgaris* 'Elstbeth'; GST, glandular secretory trichome. White frames in (b) and (e) represent 0.4 mm × 0.4 mm.

**(B)** The density of glandular secretory trichomes is shown in TqLeaf and TvELeaf by scanning electron microscopy. (a) Tq, *T. quinquecostatus*. (b) TvE, *T. vulgaris* 'Elstbeth'. The yellow stars indicate glandular secretory trichomes.

**(C)** Glandular secretory trichome type and developmental pathway in thyme. CGT, capitate glandular trichome; PGT, peltate glandular trichome; NGT, nonglandular trichomes.

**(D)** Expression heatmap of DEGs in the HD-ZIP-encoding gene family. HD-ZIP, homeodomain-leucine zipper; DEGs, differentially expressed genes.

Showed that *Tq12G014160.1*, *Tq03G019480.1*, *Tq08G011440.1*, *Tq07G006560.1*, and *Tq02G008300.1* might be R2R3-MYBs, whereas *Tq05G008130.1*, *Tq04G024290.1*, *Tq07G000520.1*, *Tq07G008780.1*, *Tq01G004800.1*, *Tq10G010680.1*, *Tq03G017440.1*, *Tq05G022030.1*, *Tq06G008250.1*, and *Tq10G005330.1* might be HD-ZIP IVs (Supplemental Figure 14C). Because glandular secretory trichomes are

distributed mainly in leaves and flowers, the expression of *Tq01G004800.1*, *Tq03G017440.1*, *Tq04G024290.1*, *Tq05G008130.1*, *Tq05G022030.1*, *Tq06G008250.1*, *Tq07G000520.1*, *Tq07G008780.1*, and *Tq10G005330.1* was particularly high in these organs. These genes encode members of the HD-ZIP IV family that are likely to be related to glandular secretory trichome development in thyme.

### The genetic mechanism underlying monoterpenoid biosynthesis, identification of terpenoid-related gene expression patterns, and $\gamma$ -terpinene synthase

We measured volatiles from roots, stems, leaves, and flowers at different stages (bud, half-open, and full-open) in *T. quinquecostatus* (Figure 1B–1G) and *T. vulgaris* ‘Elsbeth’ using headspace solid-phase microextraction coupled to gas chromatography-mass spectrometry (HS-SPME-GC-MS). The composition and content of volatile organic compounds (VOCs) differed between the two species. The absolute contents of thymol, carvacrol, *p*-cymene,  $\gamma$ -terpinene,  $\alpha$ -terpinene, 1,8-cineole, *trans*- $\beta$ -ocimene, and endo-borneol were relatively high. VOCs in flowers were higher than those in leaves. Furthermore, VOCs in the bud stage were higher than those in the other flower developmental stages and decreased gradually as the flowers opened (Figure 5A). The mass spectra of major VOCs are shown in Figure 5C, and the chemical standards are shown in Supplemental Figure 15. Results of VOC analysis in *T. quinquecostatus* and *T. vulgaris* ‘Elsbeth’ were similar to those in other plant species. For example, VOCs in *Cistanche deserticola* flower buds gradually decreased or disappeared with flowering (Qiao et al., 2021). Li et al., 2019 found that 14 VOCs accumulated in lavender flower buds and decreased as the flowers matured. In the red apple ‘Pelingo,’ linalool was the most abundant flower volatile, accounting for 43% of volatiles in the flower buds and 27.7% in the mature flowers (Fraternale et al., 2014). Among essential oil constituents, the phenolic monoterpenes thymol and its isomer carvacrol, along with their biogenetic precursors *p*-cymene and  $\gamma$ -terpinene, are the most frequent chemophenetic and bioactive markers in several *Thymus* species (Morshedloo et al., 2017; Emami Bistgani et al., 2018).

The monoterpenoid biosynthetic pathway of *T. quinquecostatus* is shown in Figure 5B. A diverse array of differentially expressed genes (DEGs) in the MEP pathway, including members of eight gene families and 13 DEGs encoding four 1-deoxy-D-xylulose 5-phosphate synthases (DXSs), one 1-deoxy-D-xylulose 5-phosphate reductoisomerase (DXR), one 2-C-methyl-derythritol-4-phosphate cytidylyltransferase (MCT), one 4-(cytidine-5-diphospho)-2-C-methyl-D-erythritol kinase (CMK), one 2-C-methyl-D-erythritol-2,4-cyclodiphosphate synthase (MDS), two (E)-4-hydroxy-3-methyl-but-2-enyl-pyrophosphate reductases (HDSs), two isopentenyl diphosphate isomerasers (IDIs), and one geranyl diphosphate synthase (GPPS), were identified in the *T. quinquecostatus* genome (Figure 5B). Our results showed that the copy numbers of these genes were expanded in thyme, especially for DXS, which encodes the crucial rate-limiting enzyme of the MEP pathway.

TPSs catalyze the formation of the basic skeleton of monoterpenes (C10) from GPP. We identified 36 DEGs encoding TPSs, which catalyze the synthesis of  $\gamma$ -terpinene,  $\alpha$ -terpineol, borneol, and ocimene (Figure 5B). Phylogenetic tree analysis of TPS-encoding DEGs in *T. quinquecostatus* and other species showed that *Tq02G002290.1* and *Tq13G005250.1* may be  $\gamma$ -terpinene synthase-encoding genes (Figure 6C). TPS-, CYP-, and SDR-encoding genes are crucial for monoterpenoid biosynthesis and are often found in physical clusters in the genome (Supplemental Table 16). Sequence similarity results showed that 69, 420, and

163 TPS-, CYP-, and SDR-encoding genes were present in *T. quinquecostatus*. Furthermore, we identified 189 differentially expressed CYP-encoding genes and 47 SDR-encoding genes, which catalyze the formation of carvacrol and thymol from *p*-cymene (Supplemental Figure 16). Phylogenetic tree analysis of CYP- and SDR-encoding DEGs in *T. quinquecostatus* and *CYP71D*s and SDRs of other species, showed that *Tq06G018730.1*, *Tq06G018750.1*, *Tq06G018720.1*, *Tq03G008200.1*, *Tq13G008670.1*, *Tq04G023650.1*, and *Tq05G002240.1* may be *CYP71D*s (Supplemental Figure 14D). On the other hand, *Tq07G003330.1*, *Tq03G029330.1*, *Tq04G008130.1*, *Tq13G017990.1*, *Tq13G002980.1*, and *Tq09G015420.1* may be SDRs (Supplemental Figure 14A). These results show that TPS-, CYP71D-, and SDR-encoding genes are key genes related to thymol and carvacrol biosynthesis and lay the foundation for future research on gene function in thyme.

We used weighted gene coexpression network analysis (WGCNA), which is a systems biology method, to analyze gene expression in thymes. Through WGCNA, we elucidated 21965 DEGs (Supplemental Figure 17A) and analyzed the relationships among modules (Supplemental Figure 17B). Using a set of parameters that produced refined clusters, we detected 17 modules containing 101–1481 DEGs each (fold change [FC] > 2 or < 0.5, false discovery rate [FDR] < 0.01) (Supplemental Figure 17B). Hub gene analyses were useful in revealing important regulatory factors and genes for monoterpenoid biosynthesis and glandular secretory trichome formation. Transcriptome data analyses and WGCNA revealed gene hubs, which were coexpressed with terpenoid- and trichome-related gene modules (Figure 6B). Among the modules were TPS-, CYP71D-, and SDR-encoding genes related to monoterpenoid biosynthesis and R2R3-MYB- and HD-ZIP IV-encoding genes associated with glandular secretory trichome formation. qRT-PCR results also showed that *Tq06G018730.1* (CYP71D), *Tq13G017990.1* (SDR), *Tq05G008130.1* (HD-ZIP IV), and *Tq12G014160.1* (R2R3-MYB) played important roles in monoterpenoid biosynthesis and glandular secretory trichome formation, consistent with the heatmap analysis of these DEGs in thymes (Supplemental Figure 18).

To identify the relationship between modules and terpenoids, gene coexpression networks were constructed using 21965 DEGs (Figure 6A). Highly interconnected genes were clustered in the same module, and 17 modules were obtained. The module-terpenoid relationship revealed that each terpenoid was significantly relevant to at least one module (Figure 6A). The investigation of relationships between 17 module eigengenes and terpenoid content revealed that the correlation coefficients ranged from -0.55 to 0.87 for  $\gamma$ -terpinene (Figure 6B). The eigengenes of the MEIndianred3, MEviolet, and MEsalmon4 modules showed significant positive correlations with  $\gamma$ -terpinene ( $R > 0.5$ ,  $p < 0.05$ ) (Figure 6B). Nine compounds showed significant correlations with MEsalmon4 and seven compounds with MEIndianred3. The compounds were negatively correlated with MEGreenyellow and MEmagenta4 and positively correlated with MEblueviolet, and vice versa. The MEIndianred3 module consisted of three TPS-encoding genes: *Tq02G002290.1*, *Tq03G009870.1*, and *Tq13G005250.1*.

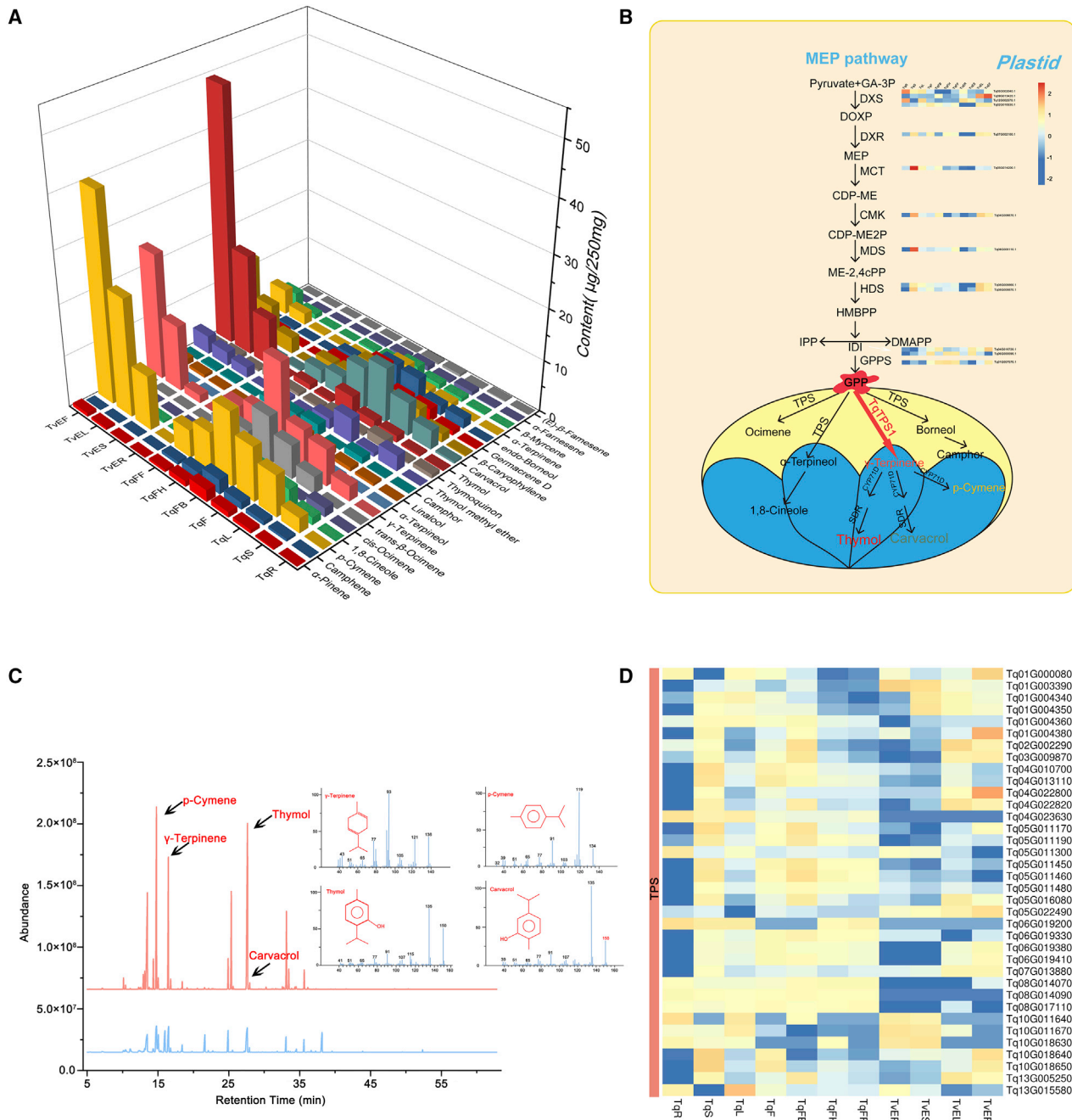


**Figure 5. Analysis of compounds in different tissues and schematic overview of the monoterpene biosynthetic pathway.**

(A) Major volatile compounds in different tissues per 250 mg in *T. vulgaris* 'Elisbeth' and *T. quinquecostatus*.

(B) Monoterpene biosynthesis in the MEP pathway.

(C) GC-MS peaks of flowers in *T. vulgaris* 'Elisbeth' (red) and *T. quinquecostatus* (blue) and the mass spectra of p-cymene, γ-terpinene, thymol, and carvacrol.

(D) Heatmap of DEGs in the TPS-encoding gene family.

To investigate the evolutionary relationship between the *Tq02G002290.1* gene identified in this study and other TPS-encoding genes, a phylogenetic tree was generated by the neighbor-joining method using amino acid sequences of TPS DEGs of *T. quinquecostatus* and other plant species. *Tq02G002290.1* clustered together with six other previously reported γ-terpinene synthase-encoding genes in oregano and thyme, such as *OvTPS2.1*, *OvTPS2.2*, *TcTPS2.1*, *TcTPS2.2*,

*TvTPS1*, and *TvTPS2* (Crocoll et al., 2010; Lima et al., 2013; Rudolph et al., 2016) (Figure 6C). Multiple alignment revealed that the amino acid sequence of the protein encoded by *Tq02G002290.1* was highly similar to those of other functionally characterized TPS proteins, and it contained conserved domains such as DDXXD and NSE/DTE. TPS enzymes catalyze steps in terpene biosynthesis by binding to  $\text{Mg}^{2+}$  or  $\text{Mn}^{2+}$  cofactors, and RRX<sub>8</sub>W is involved in cyclization reactions

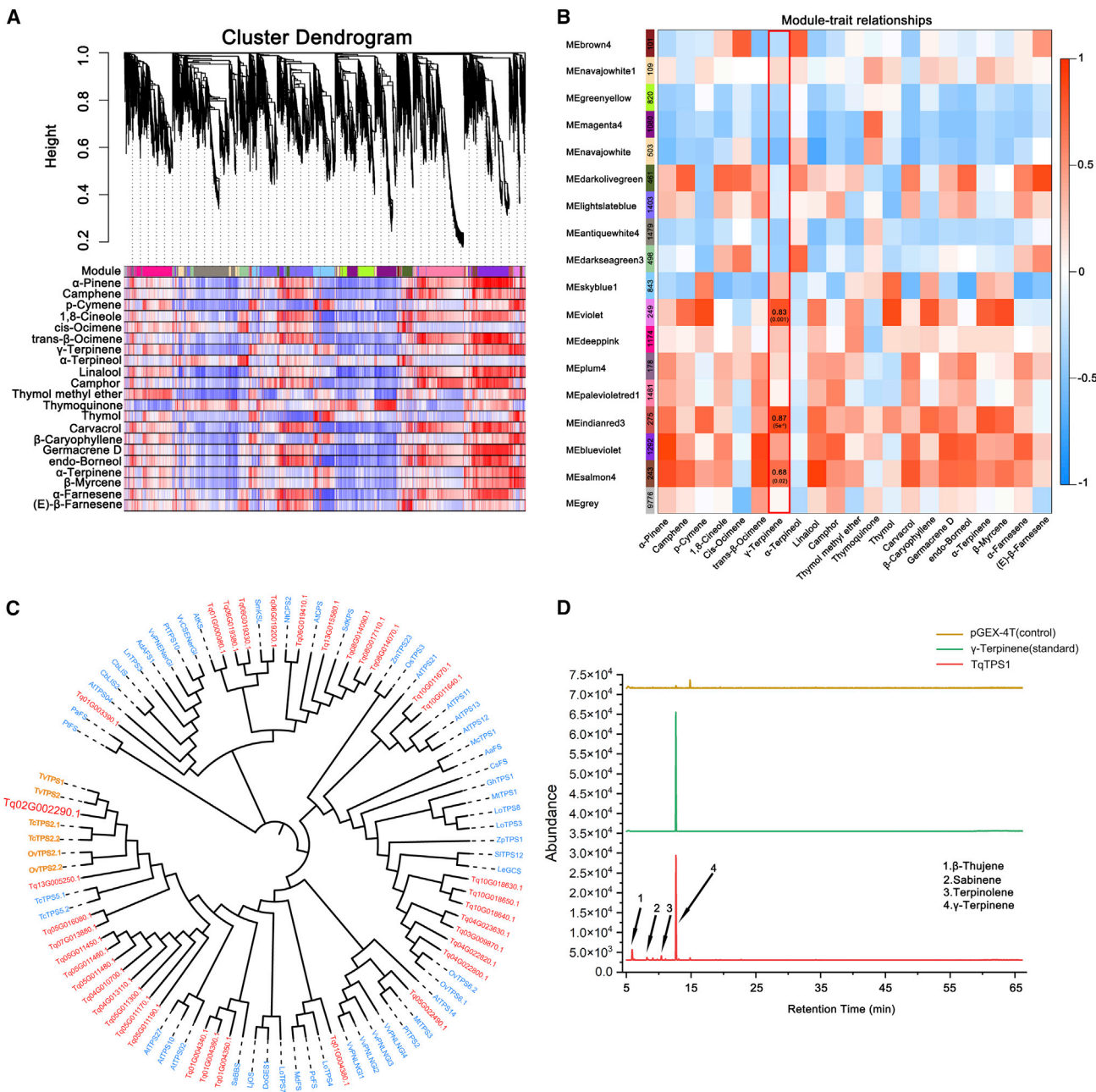


**Figure 6. Modular analysis of terpenoid-associated genes on the basis of WGCNA and  $\gamma$ -terpinene synthase-encoding gene expression analysis.**

- (A) The heatmap shows the relatedness of terpenoids with all coexpression modules identified in WGCNA.
- (B) Modular organization analysis of terpenoid-related gene expression in thyme. Module–terpenoid correlations and corresponding p values (in parenthesis). The left panel shows 17 modules. The right panel is a color scale for module trait correlation from –1 to 1.
- (C) Phylogenetic tree of the TPS-encoding genes (DEGs) in thyme and other species. *TvTPS1*, *TvTPS2*, *TcTPS2.1*, *TcTPS2.2*, *OvTPS2.1*, and *OvTPS2.2* (orange color) are  $\gamma$ -terpinene synthase-encoding genes in thyme and oregano (Lamiaceae).
- (D) Heterologous expression of *TqTPS1* in *Escherichia coli* via *in vitro* enzyme assay. WGCNA, weighted gene coexpression network analysis.

during catalysis (Supplemental Figure 19C). To confirm the activity of the *Tq02G002290.1*-encoded protein and elucidate its role in monoterpene biosynthesis in *T. quinquecostatus*, a GPP substrate was used in cell-free systems. Recombinant protein for biochemical analysis was prepared by cloning *Tq02G002290.1* and expressing it in the *Escherichia coli* BL21

strain, with the *E. coli* expression system containing empty vectors as a control (Supplemental Figure 19A). The *Tq02G002290.1* protein product was successfully induced in the supernatant and purified as a homogeneous soluble protein (Supplemental Figure 19B). The product peaks were identified by comparing mass spectra with the National Institute of

## Plant Communications

Standards and Technology (NIST) library or in relation to standards. In general, the protein encoded by *Tq02G002290.1* was found to be a versatile enzyme, yielding the main product  $\gamma$ -terpinene along with the by-products  $\beta$ -thujene, sabinene, and terpinolene. As such, *Tq02G002290.1* was named *TqTPS1* (Figure 6D). TPSs act as metabolic gatekeepers in the biosynthesis of diverse plant terpenoids (Mcgarvey and Croteau, 1995). In *Lathyrus odoratus*, five LoTPS were found to be C10/C15 multisubstrate enzymes that catalytically generated multiple volatilized terpenes (Bao et al., 2020). As mentioned above, *TqTPS1* is capable of catalyzing the formation of multiple products. However, it remains to be determined whether *TqTPS1* is a multisubstrate enzyme.

Plants in the genus *Thymus* are widely used as spices, herbal teas, and insecticides because of their flavor and fragrance. Here, we sequenced the genome of the representative Chinese native thyme *T. quinquecostatus*. The *T. quinquecostatus* genome has 13 pseudochromosomes with a total length of 528.66 Mb. Comparative genomic analyses showed that *T. quinquecostatus* had a close relationship with *O. tenuiflorum*, *S. splendens*, and *S. miltiorrhiza*. Ks and 4DTv analyses indicated that the *T. quinquecostatus* genome experienced two WGD events. In-depth analyses of the *T. quinquecostatus* genome revealed the biosynthetic pathway of monoterpene bioactive components and gene networks controlling glandular secretory trichome development, most notably *TqTPS1*. Our results provide new targets for the synthesis of downstream monoterpene biosynthetic products in thyme, such as thymol and carvacrol. The datasets and analyses presented in this study provide an important resource that will facilitate molecular breeding and functional gene identification in thyme.

## METHODS

### Plant materials

A survey of native thyme species grown in China was carried out using the Flora of China (Li and IAN, 1994). According to ethnobotanical information, all *T. quinquecostatus* (NCBI TaxID 228974) accessions were collected directly from Jinhekou village in the Hebei province of China in 2018. Herbarium specimens were identified and categorized by the Institute of Botany, Chinese Academy of Sciences (IB-CAS). *T. quinquecostatus* and *T. vulgaris* 'Elsbeth' were grown at the IB-CAS experimental farm, Beijing, China. *T. quinquecostatus* was selected for *de novo* sequencing because it is widely used as a medicinal plant in China. Fresh young leaves of *T. quinquecostatus* were collected from plants, immediately frozen in liquid nitrogen, and stored at  $-80^{\circ}\text{C}$  before DNA extraction.

### Genome sequencing

Genomic DNA was extracted from young leaves of *T. quinquecostatus* using a DNA Secure Plant Kit (Tiangen, China). An Illumina genomic library was constructed according to Illumina's standard protocol, and paired-end reads ( $2 \times 150$  bp) sequenced on an Illumina NovaSeq 6000 platform were used for genome survey and assessment. The genomes were sequenced using the PacBio Sequel II platform (Pacific Biosciences) to produce CCS reads (HiFi) for contig assembly. The Hi-C library (vanBerkum et al., 2010) was constructed using the HindIII restriction enzyme according to the instructions of the BioMarker Technologies Company (Xie et al., 2015) and sequenced on an Illumina NovaSeq 6000 platform for chromosome construction. Four types of live *T. quinquecostatus* tissues (root, stem, leaf, and flower) were collected for transcriptome sequencing for genome annotation and assessment.

### Chromosome-level genome of *Thymus quinquecostatus*

RNA-seq libraries were sequenced on an Illumina NovaSeq 6000 platform in paired-end mode. All sequencing services were provided by Biomarker Technologies Co., Ltd. (Beijing, China).

### Genome survey and assembly

The genome size, heterozygosity, and repeat content were estimated on the basis of k-mer distribution using 19-mers extracted from the Illumina short reads. The estimated genome size was further validated using flow cytometry. Raw PacBio subreads were filtered and corrected using the PacBio circular consensus sequencing (pbccs) pipeline with default parameters (<https://github.com/PacificBiosciences/ccs>). The resulting CCS reads were subjected to hifiasm (version 0.12) (Cheng et al., 2021) for *de novo* assembly. The primary contigs were corrected using Pilon software (version 1.18) (Utturkar et al., 2017). BWA (version 0.7.10-r789) (Li, 2013) and SAMtools (version 1.9) (Li et al., 2009) were used for read alignment and SAM/BAM format conversion. CEGMA (version 2.5) (Parra et al., 2007) and BUSCO (version 4) (Simão et al., 2015) were used to assess the completeness of the genome and gene annotation.

### Chromosome assembly using Hi-C

The raw data were filtered using a Perl script as implemented in LACHE-SIS software (Burton et al., 2013). BWA software (version 0.7.10-r789) (Li, 2013) was used to map the Hi-C reads to the draft assembly, and uniquely mapped reads were selected for further analysis. Our newly developed ALLHiC (Zhang et al., 2019) pipeline was used to link the contigs to 13 pseudochromosomes. HiC-Pro software (version 2.10.0) (Servant et al., 2015) was used to calculate the Hi-C mapping rate and evaluate the quality of the Hi-C scaffolding.

### Protein-coding gene prediction

The following three approaches, as incorporated in the Evidence Modeler (EVM) pipeline (version 1.1.1) (Haas et al., 2008), were used to predict high-quality protein-coding genes: *ab initio* gene predictions, transcript evidence, and homology-based predictions. Augustus (version 2.4) (Stanke et al., 2008) and SNAP (version 2006-07-28) (Korf, 2004) were used for *ab initio* gene predictions. For homology-based prediction models, six proteomes (*A. thaliana*, *O. tenuiflorum*, *S. baicalensis*, *S. miltiorrhiza*, *S. splendens*, and *T. grandis*) were downloaded from the Phytozome database (<https://phytozome.jgi.doe.gov/pz/portal.html>). The protein sequences of the *T. quinquecostatus* genome were aligned to those of the six species using GeMoMa software (version 1.7) (Keilwagen et al., 2016). For transcript evidence, RNA-seq data from different tissues (root, stem, leaf, and flower) were assembled against reference transcripts using HISAT (version 2.0.4) (Kim et al., 2015b), StringTie (version 1.2.3) (Pertea et al., 2015), and GeneMarks-T (version 5.1) (Tang et al., 2015a). The no-reference transcripts were assembled using Trinity (version 2.11) (Grabherr et al., 2011), and PASA (version 2.0.2) (Haas et al., 2003) was used for gene prediction. Finally, tiers with protein-coding evidence were incorporated in the EVM pipeline (version 1.1.1) (Haas et al., 2008) to predict high-quality protein-coding genes.

### Functional annotation

Functional annotations of protein-coding genes from *T. quinquecostatus* were obtained by performing BLASTP against the public databases EggNOG (Huerta-Cepas et al., 2019), GO (Ashburner et al., 2000), KOG (Koonin et al., 2004), TrEMBL (Boeckmann et al., 2003), nr (Marchler-Bauer et al., 2011), Swiss-Prot (Bairoch and Apweiler, 2000), and KEGG (Kanehisa et al., 2014) with an E-value cut-off of  $1.0 \times 10^{-5}$ . Protein domains were identified using InterProScan (version 4.8) (Jones et al., 2014) and HMMER (version 3.3) (Klingenberg et al., 2013) to query against the InterPro and Pfam databases. GO terms were assigned on the basis of InterPro or Pfam entries. In addition, protein-coding genes were searched against the KEGG database to identify possible pathways in which they might be involved. GO enrichment and KEGG pathway analysis were performed using the online platform OmicShare (<https://www.omicshare.com/>).

### Identification of repetitive elements

For *de novo* prediction, the repeat sequence library of the genome was first customized using the RepeatModeler2 pipeline (version 2.0.1) (Flynn et al., 2020), which used RECON (version 1.0.8) (Bao and Eddy, 2002) and RepeatScout (version 1.0.6) (Price et al., 2005) to obtain the consensus repeat library. RepeatClassifier was then used to identify and cluster repetitive elements with the Repbase (version 19.06) (Jurka et al., 2005), REXdb (version 3.0) (Neumann et al., 2019), and Dfam (version 3.2) (Wheeler et al., 2013) databases. LTR\_retriever (version 2.8) (Ou and Jiang, 2017), LTRharvest (version 1.5.9) (Ellinghaus et al., 2008), and LTR\_FINDER (version 1.1) (Xu and Wang, 2007) software packages were then used to classify the unknown-type transposon sequences (TEs). Finally, RepeatMasker (version 4.1.0) (Tarailo-Graovac and Chen, 2009) was used to predict the TEs in the genome based on the constructed repeat sequence database. The microsatellite identification tool MISA (version 2.1) (Beier et al., 2017) and the Tandem Repeat Finder version 409 (TRF) package (Benson, 1999) were used to identify tandem repeat sequences in the genome.

### Identification of noncoding RNA genes and pseudogenes

tRNAscan-SE software (version 1.3.1) (Chan and Lowe, 2019) was used with eukaryotic parameters to identify tRNA genes. Barnap (version 0.9) (Singleton et al., 2021) was used to identify rRNA genes mainly on the basis of the Rfam database (version 13.0) (Kalvari et al., 2017). The miRBase database (Griffiths-Jones et al., 2006) was used to identify miRNA genes. Infernal (version 1.1) (Nawrocki and Eddy, 2013) was used with default parameters to annotate snRNA and snoRNA genes on the basis of the Rfam database (version 13.0) (Kalvari et al., 2017). genBlastA (version 1.0.4) (She et al., 2009) and GeneWise (version 2.4.1) (Birney et al., 2004) were used to predict pseudogenes.

### Reconstruction of the phylogenetic tree

OrthoFinder (version 2.4.0) (Emms and Kelly, 2019) was used to identify homologous genes in *T. quinquecostatus* and 15 angiosperm species. MAFFT (version 7.407) (Katoh and Standley, 2013) was used with default parameters to align each orthologous gene sequence. The PANTHER version 15 database (Mi et al., 2019) was used to annotate gene families. Individual gene alignments were processed using in-house Python scripts to extract conserved regions. Conserved regions of individual genes were concatenated into a supermatrix dataset. GO and KEGG enrichment analysis was performed using unique gene families of *T. quinquecostatus* via clusterProfiler (version 3.14.0) (Yu et al., 2012). ModelFinder (Kalyaanamoorthy et al., 2017), as implemented in IQ-TREE (version 1.6.11) (Nguyen et al., 2015), was used to estimate the best substitution models. Finally, RAxML was used with the best-fit substitution model and 1000 bootstrap replicates to infer the maximum-likelihood tree. Divergence time estimates were calculated using the MCMCTree program in Phylogenetic Analysis by Maximum Likelihood software (PAML version 4.9i) (Yang, 1997), with two secondary calibration points obtained from the TimeTree database (Kumar et al., 2017) (<http://www.timetree.org/>). The graphical phylogenetic tree was displayed using MCMCTreeR (version 1.1) (Puttick, 2019).

### Expansion and contraction of gene families

All the deduced proteins were filtered using in-house Python scripts to remove alternative splicing and redundant genes, and only the longest transcripts were retained. BLASTP software was used to identify gene-family clusters via OrthoMCL (Enright et al., 2002) on the basis of sequence similarity information from the BLAST output. Based on the dated phylogeny, expansions and contractions of orthologous gene families were determined using CAFE software (version 4.2) (Han et al., 2013). Gene families were considered significantly expanded or contracted when they presented p values smaller than 0.05. Genes in significantly expanded families were then used for GO and KEGG enrichment analysis.

### Synteny analysis and whole-genome duplication

CIRCOS software (version 0.69-6) (Krzewinski et al., 2009) was used to visualize gene density, G-C content, repeats, and gene synteny on individual pseudochromosomes. BLASTP was used to examine WGD in the *T. quinquecostatus* genome and identify orthologous and paralogous genes. MCSanX software (Wang et al., 2012) was used to identify collinear blocks. Syntenic blocks were visualized using MCSan, and chromosome lengths were not scaled. Synonymous substitution rates (Ks) of the collinear orthologous gene pairs were calculated using WGD software (version 1.1.1) (Zwaenepoel and Van de Peer, 2019). The synonymous substitutions per site per year as  $8.61 \times 10^{-9} (\mu)$  were estimated using divergence time. The mean Ks values of syntenic blocks between *T. quinquecostatus* and *S. miltiorrhiza*, and two WGD events in the *T. quinquecostatus* genome, were investigated using the following equation: time = Ks/2 $\mu$ . The 4DTv value of each gene pair was calculated and then corrected using the script in the following link: <https://github.com/JinfengChen/Scripts>.

LTR sequences (set parameter S ≥ 6) in the *T. quinquecostatus* genome were identified using LTR\_FINDER (version 1.07) (Xu and Wang, 2007). Distance K was calculated using the Kimura model in EMBOSS (version 6.6.0) (Rice et al., 2000). The integration times (Mya) of intact LTRs were estimated using the following equation: T = K/2r, where K is the number of nucleotide substitutions per site between each LTR pair, and r is the nucleotide substitution rate, which was set to  $7 \times 10^{-9}$  substitutions per site per year (Ossowski et al., 2010).

DIAMOND (version 0.9.29.130) (Buchfink et al., 2015) was used to compare the gene sequences of the two species to determine similar gene pairs (E < 1e<sup>-5</sup>, C score > 0.5, where JCVI software was used to filter the C score value). Next, MCSanX (Wang et al., 2012) was used to determine whether similar gene pairs were adjacent on the chromosomes and ultimately to obtain all the genes in the syntenic block. Collinear patterns of each species were drawn using JCVI (version 0.9.13) (Tang et al., 2015b). Chromosome-scale syntenic block scattered point graphs and bar graphs were constructed using VGSC (Xu et al., 2016b).

### Phylogenetic analysis of TPS-, CYP-, SDR-, MYB-, and HD-ZIP-encoding genes

TPS-, CYP-, SDR-, MYB-, and HD-ZIP-encoding genes were identified from the scientific literature (Supplemental Tables 17–21). The amino acid sequences of the proteins encoded by these genes were obtained from the National Center for Biotechnology Information (NCBI) website (<https://www.ncbi.nlm.nih.gov/>). TPS-, CYP-, SDR-, MYB-, and HD-ZIP-encoding genes were identified using the MAKER-P pipeline (Campbell et al., 2014) and Fgenesh (Salamov and Solovyev, 2000). *T. quinquecostatus* TPS-, CYP-, SDR-, MYB-, and HD-ZIP-encoding genes were predicted using hmmscan (Finn et al., 2010) and NLR-parser (Steuernagel et al., 2015). Phylogenetic trees of DEGs and genes of other species obtained from NCBI were constructed using MEGA X (Kumar et al., 2018).

### Transcriptome sequencing, identification of specifically expressed genes, and WGCNA analysis

Raw RNA-seq data from four tissues (root, stem, leaf, and flower) of *T. quinquecostatus* and *T. vulgaris* 'Elisbeth' and three flower developmental stages (bud, half-bloom, and full-bloom) of *T. quinquecostatus* were filtered using Trimmomatic software (Bolger et al., 2014). The resulting clean reads were mapped to coding sequences predicted from the genome using Bowtie (version 2.0) (Langmead and Salzberg, 2012). Fragments per kilobase of exon per million fragments mapped (FPKM) were calculated using RSEM software (version 1.3.2) (<https://github.com/deweylab/RSEM>) implemented in Trinity (Grabherr et al., 2011). Genes with  $|\log_{2}FC| > 2$  and  $p < 0.05$  were identified as DEGs. Coexpression and module

analyses were performed using the R package WGCNA (version 1.51) for all DEGs ([Langfelder and Horvath, 2008](#)).

#### Observation and density of glandular secretory trichomes

The morphology and distribution of glandular secretory trichomes were evaluated using a stereomicroscope (Leica DVM6), fluorescence microscope (Leica DM6 B), and scanning electron microscope (S-4800; Hitachi, Tokyo, Japan). ImageJ software (<https://imagej.nih.gov/ij/>) was used to count glandular secretory trichomes and measure leaf area. Glandular secretory trichome density was calculated from three plants.

#### Analysis of volatile organic compounds by headspace solid-phase microextraction (HS-SPME)

VOCs of 33 RNA-seq samples were detected via headspace solid-phase microextraction (HS-SPME). Fresh leaf powder (0.25 g) was weighed and immediately placed into a 20-mL headspace vial (Agilent, Palo Alto, CA) containing 20  $\mu$ L of internal standard solution (1 mg/mL, 3-octanol, Cas#589-98-0; Aladdin, Shanghai, China). The vials were sealed using crimp-top caps with TFE-silicone headspace septa (Agilent). Each vial was immediately incubated at 40°C for 30 min, and then a 100- $\mu$ m poly-dimethylsiloxane-coated fiber (Supelco, Inc., Bellefonte, PA) was exposed to the headspace to absorb the volatiles for 30 min. All volatile components on the coated fiber were analyzed by gas chromatography (GC). A Model 7890A GC instrument and a 7000B mass spectrometer (Agilent) were used to perform GC-mass spectrometry (GC-MS) analysis ([Pontes et al., 2009](#)). The determination of the percentage content of each compound was based on normalization of the GC peak areas. Identification of the compounds was based on comparison of retention indices (RIs) relative to a homologous series of n-alkanes (C7-C40), mass spectra (MS) from the NIST library (version 14.0), and data from the scientific literature. Retention indices were based on the formula  $RI = 100Z + 100[RT(x) - RT(z)]/[RT(z+1) - RT(z)]$ ,  $RT(x)$ ,  $RT(z)$  and  $RT(z+1)$  for the composition, and the number of carbons  $Z$  and  $Z+1$  for the retention time of the normal alkane.

#### Quantitative real-time PCR (qRT-PCR)

Total RNA was extracted from three tissue replicates using the RNAPrep Pure Plant Kit (Tiangen Biotech, Beijing, China). Primers were designed using Primer Premier 5.0, and the sequences are listed in [Supplemental Table 22](#). qRT-PCR was performed using the ABI 7300 Real-time PCR System (Framingham, MA) with SYBR Green PCR Master Mix (TaKaRa), following procedures described previously ([Wang et al., 2015](#)). All PCR assays were performed in triplicate. The reference gene was 18S rRNA. Relative expression levels were quantified with the  $2^{-\Delta\Delta Ct}$  method ([Wang et al., 2014](#)).

#### Heterologous expression of *TqTPS1* in *Escherichia coli* and *in vitro* enzyme assay

To express *TqTPS1* recombinant proteins in *E. coli*, the full-length sequence of *TqTPS1* was amplified with precise primers and then subcloned into the pGEX 4T-1 vector system. Next, an empty vector (as a control) and vectors ligated with *TqTPS1* were transformed into *E. coli* strain BL21 (DE3). Expression of recombinant *TqTPS1* was induced using 0.5 mM isopropyl- $\beta$ -D-thiogalactopyranoside (IPTG) at 18°C for 12 h in an incubator with constant shaking. Subsequently, the cells were harvested via centrifugation, resuspended in phosphate-buffered saline, and broken down via sonication. Crude proteins were then applied to glutathione beads (Tiandirenhe Biotech, Changzhou, China). The purified protein was incubated with GPP, and the reaction product was detected using GC-MS.

#### Statistical analysis

All samples were prepared and analyzed in triplicate, and data were expressed as the mean  $\pm$  SD. Statistical analyses were performed by analysis of variance (ANOVA), and Duncan's test was used to determine the

## Chromosome-level genome of *Thymus quinquecostatus*

significance of differences between groups. Differences at  $p < 0.05$  were considered significant. SPSS 18 (SPSS Inc., Chicago, IL) was used for the analysis.

## AVAILABILITY OF DATA AND MATERIALS

The raw sequence and genome assembly data were deposited in NCBI under project accession number PRJNA690675. The genome assembly and annotation data were also deposited in the China National Genomics Data Center under project accession number GWHBJVA00000000.

## SUPPLEMENTAL INFORMATION

Supplemental information is available at *Plant Communications Online*.

## FUNDING

This work was supported by the Strategic Priority Research Program of the Chinese Academy of Sciences (grant XDA23080603).

## AUTHOR CONTRIBUTIONS

M.S. and Y.Z. performed the experiments, analyzed the data, and wrote the manuscript. L.Z. and N.L. helped with thyme VOC analysis. H.B. and G.S. helped with sample collection and analyzed the data. J.Z. helped with sample collection and research design. L.S. was involved in designing the research and revising the manuscript. All authors read and approved the manuscript.

## ACKNOWLEDGMENTS

We thank Professor Cathie Martin from the John Innes Center of Norwich Research Park in the UK and Dr. Qing Zhao from the Shanghai Chenshan Botanical Garden of the Chinese Academy of Sciences in China for sharing the *Scutellaria baicalensis* genome-wide annotation files. No conflict of interest declared.

Received: February 27, 2022

Revised: June 19, 2022

Accepted: July 11, 2022

Published: July 16, 2022

## REFERENCES

- Afendi, F.M., Okada, T., Yamazaki, M., Hirai-Morita, A., Nakamura, Y., Nakamura, K., Ikeda, S., Takahashi, H., Altaf-Ul-Amin, M., Darusman, L.K., et al.** (2012). KNApSACk family databases: integrated metabolite-plant species databases for multifaceted plant research. *Plant Cell Physiol.* **53**:e1.
- Ashburner, M., Ball, C.A., Blake, J.A., Botstein, D., Butler, H., Cherry, J.M., Davis, A.P., Dolinski, K., Dwight, S.S., Eppig, J.T., et al.** (2000). Gene ontology: tool for the unification of biology. *Nat. Genet.* **25**:25–29.
- Bairoch, A., and Apweiler, R.** (2000). The SWISS-PROT protein sequence database and its supplement TrEMBL in 2000. *Nucleic Acids Res.* **28**:45–48.
- Bao, T., Shadrack, K., Yang, S., Xue, X., Li, S., Wang, N., Wang, Q., Wang, L., Gao, X., and Cronk, Q.** (2020). Functional characterization of terpene synthases accounting for the volatilized-terpene heterogeneity in *Lathyrus odoratus* cultivar flowers. *Plant Cell Physiol.* **61**:1733–1749.
- Bao, Z., and Eddy, S.R.** (2002). Automated de novo identification of repeat sequence families in sequenced genomes. *Genome Res.* **12**:1269–1276.
- Behnaz, T., Mehdi, R., Ahmad, A., and Helena, T.** (2020). Sequencing and variation of terpene synthase gene (TPS2) as the major gene in biosynthesis of thymol in different Thymus Species. *Phytochemistry* **169**:112126.

- Beier, S., Thiel, T., Münch, T., Scholz, U., and Mascher, M.** (2017). Misa-web: a web server for microsatellite prediction. *Bioinformatics* **33**:2583–2585.
- Benelli, G., Pavela, R., Canale, A., Cianfaglione, K., Ciaschetti, G., Conti, F., Nicoletti, M., Senthil-Nathan, S., Mehlhorn, H., and Maggi, F.** (2017). Acute larvicidal toxicity of five essential oils (*Pinus nigra*, *Hyssopus officinalis*, *Satureja montana*, *Aloysia citrodora* and *Pelargonium graveolens*) against the filariasis vector *Culex quinquefasciatus*: synergistic and antagonistic effects. *Parasitol. Int.* **66**:166–171.
- Benson, G.** (1999). Tandem repeats finder: a program to analyze DNA sequences. *Nucleic Acids Res.* **27**:573–580.
- Birney, E., Clamp, M., and Durbin, R.** (2004). GeneWise and genomewise. *Genome Res.* **14**:988–995.
- Boeckmann, B., Bairoch, A., Apweiler, R., Blatter, M.C., Estreicher, A., Gasteiger, E., Martin, M.J., Michoud, K., O'Donovan, C., Phan, I., et al.** (2003). The SWISS-PROT protein knowledgebase and its supplement TrEMBL in 2003. *Nucleic Acids Res.* **31**:365–370.
- Bolger, A.M., Lohse, M., and Usadel, B.** (2014). Trimmomatic: a flexible trimmer for illumina sequence data. *Bioinformatics* **30**:2114–2120.
- Buchfink, B., Xie, C., and Huson, D.H.** (2015). Fast and sensitive protein alignment using DIAMOND. *Nat. Methods* **12**:59–60.
- Burton, J.N., Adey, A., Patwardhan, R.P., Qiu, R., Kitzman, J.O., and Shendure, J.** (2013). Chromosome-scale scaffolding of *de novo* genome assemblies based on chromatin interactions. *Nat. Biotechnol.* **31**:1119–1125.
- Campbell, M.S., Law, M., Holt, C., Stein, J.C., Moghe, G.D., Hufnagel, D.E., Lei, J., Achawanantakun, R., Jiao, D., Lawrence, C.J., et al.** (2014). MAKER-P: a tool kit for the rapid creation, management, and quality control of plant genome annotations. *Plant Physiol.* **164**:513–524.
- Chalvin, C., Drevensek, S., Dron, M., Bendahmane, A., and Boualem, A.** (2020). Genetic control of glandular trichome development. *Trends Plant Sci.* **25**:477–487.
- Chan, P.P., and Lowe, T.M.** (2019). tRNAscan-SE: searching for tRNA genes in genomic sequences. *Methods Mol. Biol.* **1962**:1–14.
- Chan, W.K., Tan, L.T.H., Chan, K.G., Lee, L.H., and Goh, B.H.** (2016). Nerolidol: a sesquiterpene alcohol with multi-faceted pharmacological and biological activities. *Molecules* **21**:529.
- Chang, J., Yu, T., Yang, Q., Li, C., Xiong, C., Gao, S., Xie, Q., Zheng, F., Li, H., Tian, Z., et al.** (2018). Hair, encoding a single C2H2 zinc-finger protein, regulates multicellular trichome formation in tomato. *Plant J.* **96**:90–102.
- Chen, Y., Su, D., Li, J., Ying, S., Deng, H., He, X., Zhu, Y., Li, Y., Chen, Y., Pirrello, J., et al.** (2020). Overexpression of bHLH95, a basic helix-loop-helix transcription factor family member, impacts trichome formation via regulating gibberellin biosynthesis in tomato. *J. Exp. Bot.* **71**:3450–3462.
- Cheng, H., Concepcion, G.T., Feng, X., Zhang, H., and Li, H.** (2021). Haplotype-resolved *de novo* assembly using phased assembly graphs with hifiasm. *Nat. Methods* **18**:170–175.
- Crocoll, C., Asbach, J., Novak, J., Gershenson, J., and Degenhardt, J.** (2010). Terpene synthases of oregano (*Origanum vulgare* L.) and their roles in the pathway and regulation of terpene biosynthesis. *Plant Mol. Biol.* **73**:587–603.
- Dong, A.X., Xin, H.B., Li, Z.J., Liu, H., Sun, Y.Q., Nie, S., Zhao, Z.N., Cui, R.F., Zhang, R.G., Yun, Q.Z., et al.** (2018). High-quality assembly of the reference genome for scarlet sage, *Salvia splendens*, an economically important ornamental plant. *GigaScience* **7**.
- Dudareva, N., and Pichersky, E.** (2008). Metabolic engineering of plant volatiles. *Curr. Opin. Biotechnol.* **19**:181–189.
- Ellinghaus, D., Kurtz, S., and Willhöft, U.** (2008). LTRharvest, an efficient and flexible software for *de novo* detection of LTR retrotransposons. *BMC Bioinf.* **9**:18.
- Emami Bistgani, Z., Ataollah Siadat, S., Bakhshandeh, A., Ghasemi Pirbalouti, A., Hashemi, M., Maggi, F., and Reza Morshedloo, M.** (2018). Application of combined fertilizers improves biomass, essential oil yield, aroma profile, and antioxidant properties of *Thymus daenensis* Celak. *Ind. Crops Prod.* **121**:434–440.
- Emms, D.M., and Kelly, S.** (2019). OrthoFinder: phylogenetic orthology inference for comparative genomics. *Genome Biol.* **20**:238.
- Enright, A.J., Van Dongen, S., and Ouzounis, C.A.** (2002). An efficient algorithm for large-scale detection of protein families. *Nucleic Acids Res.* **30**:1575–1584.
- Finn, R.D., Mistry, J., Tate, J., Coggill, P., Heger, A., Pollington, J.E., Gavin, O.L., Gunasekaran, P., Ceric, G., Forslund, K., et al.** (2010). The Pfam protein families database. *Nucleic Acids Res.* **38**:D211–D222.
- Flynn, J.M., Hubley, R., Goubert, C., Rosen, J., Clark, A.G., Feschotte, C., and Smit, A.F.** (2020). RepeatModeler2 for automated genomic discovery of transposable element families. *Proc. Natl. Acad. Sci. USA* **117**:9451–9457.
- Fraternale, D., Flaminii, G., Ricci, D., and Giomaro, G.** (2014). Flowers volatile profile of a rare red apple tree from Marche region (Italy). *J. Oleo Sci.* **63**:1195–1201.
- Gavarić, N., Kladar, N., Mišan, A., Nikolić, A., Samoiljk, I., Mimica-Dukić, N., and Božin, B.** (2015). Postdistillation waste material of thyme (*Thymus vulgaris* L., Lamiaceae) as a potential source of biologically active compounds. *Ind. Crops Prod.* **74**:457–464.
- Grabherr, M.G., Haas, B.J., Yassour, M., Levin, J.Z., Thompson, D.A., Amit, I., Adiconis, X., Fan, L., Raychowdhury, R., Zeng, Q., et al.** (2011). Trinity: reconstructing a full-length transcriptome without a genome from RNA-Seq data. *Nat. Biotechnol.* **29**:644–652.
- Griffiths-Jones, S., Grocock, R.J., van Dongen, S., Bateman, A., and Enright, A.J.** (2006). miRBase: microRNA sequences, targets and gene nomenclature. *Nucleic Acids Res.* **34**:D140–D144.
- Haas, B.J., Delcher, A.L., Mount, S.M., Wortman, J.R., Smith, R.K., Hannick, L.I., Maiti, R., Ronning, C.M., Rusch, D.B., Town, C.D., et al.** (2003). Improving the *Arabidopsis* genome annotation using maximal transcript alignment assemblies. *Nucleic Acids Res.* **31**:5654–5666.
- Haas, B.J., Salzberg, S.L., Zhu, W., Pertea, M., Allen, J.E., Orvis, J., White, O., Buell, C.R., and Wortman, J.R.** (2008). Automated eukaryotic gene structure annotation using EvidenceModeler and the program to assemble spliced alignments. *Genome Biol.* **9**:R7.
- Han, M.V., Thomas, G.W.C., Lugo-Martinez, J., and Hahn, M.W.** (2013). Estimating gene gain and loss rates in the presence of error in genome assembly and annotation using CAFE 3. *Mol. Biol. Evol.* **30**:1987–1997.
- Hong, J.Y., Kim, H., Jeon, W.J., Baek, S., and Ha, I.H.** (2020). Antioxidative effects of *Thymus quinquecostatus* Celak through mitochondrial biogenesis improvement in RAW 264.7 macrophages. *Antioxidants* **9**:548.
- Huchelmann, A., Boutry, M., and Hachez, C.** (2017). Plant glandular trichomes: natural cell factories of high biotechnological interest. *Plant Physiol.* **175**:6–22.
- Huerta-Cepas, J., Szklarczyk, D., Heller, D., Hernández-Plaza, A., Forslund, S.K., Cook, H., Mende, D.R., Letunic, I., Rattei, T., Jensen, L.J., et al.** (2019). eggNOG 5.0: a hierarchical, functionally and phylogenetically annotated orthology resource based on 5090 organisms and 2502 viruses. *Nucleic Acids Res.* **47**:D309–D314.
- Jones, P., Binns, D., Chang, H.Y., Fraser, M., Li, W., McAnulla, C., McWilliam, H., Maslen, J., Mitchell, A., Nuka, G., et al.** (2014).

## Plant Communications

- InterProScan 5: genome-scale protein function classification. *Bioinformatics* **30**:1236–1240.
- Jurka, J., Kapitonov, V.V., Pavlicek, A., Klonowski, P., Kohany, O., and Walichiewicz, J. (2005). Repbase update, a database of eukaryotic repetitive elements. *Cytogenet. Genome Res.* **110**:462–467.
- Kalvari, I., Argasinska, J., Quinones-Olvera, N., Nawrocki, E.P., Rivas, E., Eddy, S.R., Bateman, A., Finn, R.D., and Petrov, A.I. (2017). Rfam 13.0: shifting to a genome-centric resource for non-coding RNA families. *Nucleic Acids Res.* **46**:D335–D342.
- Kalyaanamoorthy, S., Minh, B.Q., Wong, T.K.F., von Haeseler, A., and Jermiin, L.S. (2017). ModelFinder: fast model selection for accurate phylogenetic estimates. *Nat. Methods* **14**:587–589.
- Kanehisa, M., Goto, S., Sato, Y., Kawashima, M., Furumichi, M., and Tanabe, M. (2014). Data, information, knowledge and principle: back to metabolism in KEGG. *Nucleic Acids Res.* **42**:D199–D205.
- Katoh, K., and Standley, D.M. (2013). MAFFT multiple sequence alignment software version 7: improvements in performance and usability. *Mol. Biol. Evol.* **30**:772–780.
- Keilwagen, J., Wenk, M., Erickson, J.L., Schattat, M.H., Grau, J., and Hartung, F. (2016). Using intron position conservation for homology-based gene prediction. *Nucleic Acids Res.* **44**:e89.
- Kidwell, M.G., and Lisch, D. (1997). Transposable elements as sources of variation in animals and plants. *Proc. Natl. Acad. Sci. USA* **94**:7704–7711.
- Kim, D., Langmead, B., and Salzberg, S.L. (2015b). HISAT: a fast spliced aligner with low memory requirements. *Nat. Methods* **12**:357–360.
- Kim, Y.S., Hwang, J.W., Sung, S.H., Park, S.J., Kim, Y.T., Kim, E.K., Moon, S.H., Jeon, B.T., and Park, P.J. (2015a). Protective effect of carvacrol from *Thymus quinquecostatus* Celak against tert-butyl hydroperoxide-induced oxidative damage in Chang cells. *Food Sci. Biotechnol.* **24**:735–741.
- Klingenberg, H., Abhauer, K.P., Lingner, T., and Meinicke, P. (2013). Protein signature-based estimation of metagenomic abundances including all domains of life and viruses. *Bioinformatics* **29**:973–980.
- Koonin, E.V., Fedorova, N.D., Jackson, J.D., Jacobs, A.R., Krylov, D.M., Makarova, K.S., Mazumder, R., Mekhedov, S.L., Nikolskaya, A.N., Rao, B.S., et al. (2004). A comprehensive evolutionary classification of proteins encoded in complete eukaryotic genomes. *Genome Biol.* **5**:R7.
- Korf, I. (2004). Gene finding in novel genomes. *BMC Bioinf.* **5**:59.
- Kou, O., Walia, S., and Dhaliwal, G.S. (2008). Essential oils as green pesticides: potential and constraints. *Biopestic. Int.* **4**:63–84.
- Krause, S.T., Liao, P., Crocoll, C., Boachon, B., Förster, C., Leidecker, F., Wiese, N., Zhao, D., Wood, J.C., Buell, C.R., et al. (2021). The biosynthesis of thymol, carvacrol, and thymohydroquinone in Lamiaceae proceeds via cytochrome P450s and a short-chain dehydrogenase. *Proc. Natl. Acad. Sci. USA* **118**. e2110092118.
- Krzywinski, M., Schein, J., Birol, I., Connors, J., Gascoyne, R., Horsman, D., Jones, S.J., and Marra, M.A. (2009). Circos: an information aesthetic for comparative genomics. *Genome Res.* **19**:1639–1645.
- Kumar, S., Stecher, G., Li, M., Knyaz, C., and Tamura, K. (2018). Mega X: molecular evolutionary genetics analysis across computing platforms. *Mol. Biol. Evol.* **35**:1547–1549.
- Kumar, S., Stecher, G., Suleski, M., and Hedges, S.B. (2017). TimeTree: a resource for timelines, timetrees, and divergence times. *Mol. Biol. Evol.* **34**:1812–1819.
- Langfelder, P., and Horvath, S. (2008). WGCNA: an R package for weighted correlation network analysis. *BMC Bioinf.* **9**:559.
- Langmead, B., and Salzberg, S.L. (2012). Fast gapped-read alignment with Bowtie 2. *Nat. Methods* **9**:357–359.
- Li, H. (2013). Aligning sequence reads, clone sequences and assembly contigs with BWA-MEM. Preprint at arXiv. <https://doi.org/10.48550/arXiv.1303.3997>.
- Li, H., Handsaker, B., Wysoker, A., Fennell, T., Ruan, J., Homer, N., Marth, G., Abecasis, G., and Durbin, R.; 1000 Genome project data processing Supgroup (2009). The sequence alignment/map format and SAMtools. *Bioinformatics* **25**:2078–2079.
- Li, H., Li, J., Dong, Y., Hao, H., Ling, Z., Bai, H., Wang, H., Cui, H., and Shi, L. (2019). Time-series transcriptome provides insights into the gene regulation network involved in the volatile terpenoid metabolism during the flower development of lavender. *BMC Plant Biol.* **19**:313.
- Li, J., Wang, Y., Dong, Y., Zhang, W., Wang, D., Bai, H., Li, K., Li, H., and Shi, L. (2021). The chromosome-based lavender genome provides new insights into Lamiaceae evolution and terpenoid biosynthesis. *Hortic. Res.* **8**:53.
- Li, X.W., and Ian, C.H. (1994). In *Flora of China*, 17 (Science Press (Beijing) and Missouri Botanical Garden Press), pp. 186–188.
- Lima, A.S., Schimmel, J., Lukas, B., Novak, J., Barroso, J.G., Figueiredo, A.C., Pedro, L.G., Degenhardt, J., and Trindade, H. (2013). Genomic characterization, molecular cloning and expression analysis of two terpene synthases from *Thymus caespititus* (Lamiaceae). *Planta* **238**:191–204.
- Liu, Y., Liu, D., Khan, A.R., Liu, B., Wu, M., Huang, L., Wu, J., Song, G., Ni, H., Ying, H., et al. (2018). NbGIS regulates glandular trichome initiation through GA signaling in tobacco. *Plant Mol. Biol.* **98**:153–167.
- Lockton, S., and Gaut, B.S. (2005). Plant conserved non-coding sequences and parologue evolution. *Trends Genet.* **21**:60–65.
- Maes, L., and Goossens, A. (2010). Hormone-mediated promotion of trichome initiation in plants is conserved but utilizes species- and trichome-specific regulatory mechanisms. *Plant Signal. Behav.* **5**:205–207.
- Maleci, B.L., and Giuliani, C. (2006). The glandular trichomes of the Labiatae. A review. In *Proceedings of the First International Symposium on the Labiatae: Advances in Production, Biotechnology and Utilisation*, C. Cervelli, B. Ruffoni, and G.C. Dalla, eds. (Leuven, Belgium: International Society for Horticultural Science (ISHS)), pp. 85–90. *Acta Horticulturae* 723.
- Marchler-Bauer, A., Lu, S., Anderson, J.B., Chitsaz, F., Derbyshire, M.K., DeWeese-Scott, C., Fong, J.H., Geer, L.Y., Geer, R.C., Gonzales, N.R., et al. (2011). CDD: a Conserved Domain Database for the functional annotation of proteins. *Nucleic Acids Res.* **39**:D225–D229.
- Matías-Hernández, L., Jiang, W., Yang, K., Tang, K., Brodelius, P.E., and Pelaz, S. (2017). AaMYB1 and its orthologue AtMYB61 affect terpene metabolism and trichome development in *Artemisia annua* and *Arabidopsis thaliana*. *Plant J.* **90**:520–534.
- McGarvey, D.J., and Croteau, R. (1995). Terpenoid metabolism. *Plant Cell* **7**:1015–1026.
- Mi, H., Muruganujan, A., Ebert, D., Huang, X., and Thomas, P.D. (2019). PANTHER version 14: more genomes, a new PANTHER GO-slim and improvements in enrichment analysis tools. *Nucleic Acids Res.* **47**:D419–D426.
- Morshedloo, M.R., Craker, L.E., Salami, A., Nazeri, V., Sang, H., and Maggi, F. (2017). Effect of prolonged water stress on essential oil content, compositions and gene expression patterns of mono-and sesquiterpene synthesis in two oregano (*Origanum vulgare* L.) subspecies. *Plant Physiol. Biochem.* **111**:119–128.
- Nawrocki, E.P., and Eddy, S.R. (2013). Infernal 1.1: 100-fold faster RNA homology searches. *Bioinformatics* **29**:2933–2935.
- Neumann, P., Novák, P., Hošťáková, N., and Macas, J. (2019). Systematic survey of plant LTR-retrotransposons elucidates

## Chromosome-level genome of *Thymus quinquecostatus*

## Chromosome-level genome of *Thymus quinquecostatus*

- phylogenetic relationships of their polyprotein domains and provides a reference for element classification. *Mob. DNA* **10**:1.
- Nguyen, L.T., Schmidt, H.A., von Haeseler, A., and Minh, B.Q.** (2015). IQ-TREE: a fast and effective stochastic algorithm for estimating maximum-likelihood phylogenies. *Mol. Biol. Evol.* **32**:268–274.
- Ossowski, S., Schneeberger, K., Lucas-Lledó, J.I., Warthmann, N., Clark, R.M., Shaw, R.G., Weigel, D., and Lynch, M.** (2010). The rate and molecular spectrum of spontaneous mutations in *Arabidopsis thaliana*. *Science* **327**:92–94.
- Ou, S., and Jiang, N.** (2017). LTR\_retriever: a highly accurate and sensitive program for identification of long terminal-repeat retrotransposons. *Plant Physiol.* **176**:1410–1422.
- Parra, G., Bradnam, K., and Korf, I.** (2007). CEGMA: a pipeline to accurately annotate core genes in eukaryotic genomes. *Bioinformatics* **23**:1061–1067.
- Pavela, R., Maggi, F., Cianfaglione, K., Bruno, M., and Benelli, G.** (2018). Larvicidal activity of essential oils of five Apiaceae taxa and some of their main constituents against *Culex quinquefasciatus*. *Chem. Biodivers.* **15**:e1700382.
- Pertea, M., Pertea, G.M., Antonescu, C.M., Chang, T.C., Mendell, J.T., and Salzberg, S.L.** (2015). StringTie enables improved reconstruction of a transcriptome from RNA-seq reads. *Nat. Biotechnol.* **33**:290–295.
- Pontes, M., Marques, J.C., and Câmara, J.** (2009). Headspace solid-phase microextraction-gas chromatography-quadrupole mass spectrometric methodology for the establishment of the volatile composition of *Passiflora* fruit species. *Microchem. J.* **93**:1–11.
- Price, A.L., Jones, N.C., and Pevzner, P.A.** (2005). *De novo* identification of repeat families in large genomes. *Bioinformatics* **21**:i351–i358.
- Puttick, M.N.** (2019). MCMCTreeR: functions to prepare MCMCTree analyses and visualize posterior ages on trees. *Bioinformatics* **35**:5321–5322.
- Qiao, H.L., Lu, P.F., Xu, R., Chen, J., Wang, X., Ma, W.S., and Liu, T.N.** (2012). Analysis of volatile compounds of inflorescence by GC-MS from *Cistanche deserticola*. *J. Chin. Med. Mater.* **35**:573–577.
- Rice, P., Longden, I., and Bleasby, A.** (2000). EMBOSS: the European molecular biology open software suite. *Trends Genet.* **16**:276–277.
- Robert, S., and Tissier, A.** (2020). Glandular trichomes: micro-organs with model status? *New Phytol.* **225**:2251–2266.
- Rudolph, K., Parthier, C., Egerer-Sieber, C., Geiger, D., Muller, Y.A., Kreis, W., and Müller-Uri, F.** (2016). Expression, crystallization and structure elucidation of  $\gamma$ -terpinene synthase from *Thymus vulgaris*. *Acta Crystallogr. F Struct. Biol. Commun.* **72**:16–23.
- Salamov, A.A., and Solovyev, V.V.** (2000). Ab initio gene finding in *Drosophila* genomic DNA. *Genome Res.* **10**:516–522.
- Servant, N., Varoquaux, N., Lajoie, B.R., Viara, E., Chen, C.J., Vert, J.P., Heard, E., Dekker, J., and Barillot, E.** (2015). HiC-Pro: an optimized and flexible pipeline for Hi-C data processing. *Genome Biol.* **16**:259.
- She, R., Chu, J.S.C., Wang, K., Pei, J., and Chen, N.** (2009). GenBlastA: enabling BLAST to identify homologous gene sequences. *Genome Res.* **19**:143–149.
- Shi, P., Fu, X., Shen, Q., Liu, M., Pan, Q., Tang, Y., Jiang, W., Lv, Z., Yan, T., Ma, Y., et al.** (2018). The roles of AaMIXTA1 in regulating the initiation of glandular trichomes and cuticle biosynthesis in *Artemisia annua*. *New Phytol.* **217**:261–276.
- Simão, F.A., Waterhouse, R.M., Ioannidis, P., Kriventseva, E.V., and Zdobnov, E.M.** (2015). BUSCO: assessing genome assembly and annotation completeness with single-copy orthologs. *Bioinformatics* **31**:3210–3212.
- Singleton, C.M., Petriglieri, F., Kristensen, J.M., Kirkegaard, R.H., Michaelsen, T.Y., Andersen, M.H., Kondrotaite, Z., Karst, S.M.,**

## Plant Communications

- Dueholm, M.S., Nielsen, P.H., et al.** (2021). Connecting structure to function with the recovery of over 1000 high-quality metagenome-assembled genomes from activated sludge using long-read sequencing. *Nat. Commun.* **12**:2009.
- Stahl-Biskup, E., and Venskutonis, R.P.** (2012). In *Handbook of herbs and spices*, 1, Second edition (Woodhead Publishing Series in Food Science, Technology and Nutrition), pp. 499–525.
- Stanke, M., Diekhans, M., Baertsch, R., and Haussler, D.** (2008). Using native and syntenically mapped cDNA alignments to improve *de novo* gene finding. *Bioinformatics* **24**:637–644.
- Steuernagel, B., Jupe, F., Witek, K., Jones, J.D.G., and Wulff, B.B.H.** (2015). NLR-parser: rapid annotation of plant NLR complements. *Bioinformatics* **31**:1665–1667.
- Tak, J.H., and Isman, M.B.** (2016). Metabolismof citral, the major constituent of lemongrass oil, in the cabbage looper, *Trichoplusia ni*, and effects of enzyme inhibitors on toxicity and metabolism. *Pestic. Biochem. Physiol.* **133**:20–25.
- Tang, H.B., Krishnakumar, V., Li, J.P., Kim, M., and Zhang, X.T.** (2015b). jcvi: JCVI utility libraries. Preprint at Zenodo. <https://doi.org/10.5281/zenodo.31631>.
- Tang, S., Lomsadze, A., and Borodovsky, M.** (2015a). Identification of protein coding regions in RNA transcripts. *Nucleic Acids Res.* **43**:e78.
- Tarailo-Graovac, M., and Chen, N.** (2009). Using RepeatMasker to identify repetitive elements in genomic sequences. *Curr. Protoc. Bioinf.* **4**:4–10.
- Tholl, D.** (2006). Terpene synthases and the regulation, diversity and biological roles of terpene metabolism. *Curr. Opin. Plant Biol.* **9**:297–304.
- Tissier, A.** (2012). Glandular trichomes: what comes after expressed sequence tags? *Plant J.* **70**:51–68.
- Utturkar, S.M., Klingeman, D.M., Hurt, R.A., and Brown, S.D.** (2017). A case study into microbial genome assembly gap sequences and finishing strategies. *Front. Microbiol.* **8**:1272.
- van Berkum, N.L., Lieberman-Aiden, E., Williams, L., Imakaev, M., Gnirke, A., Mirny, L.A., Dekker, J., and Lander, E.S.** (2010). Hi-C: a method to study the three-dimensional architecture of genomes. *J. Vis. Exp.* **39**:1869.
- Wang, H.Y., Park, S., Kim, S., Lee, D., Kim, G., Kim, Y., Park, K.H., and Lee, H.** (2015). Use of hTERT and HPV E6/E7 mRNA RT-qPCR TaqMan assays in combination for diagnosing high-grade cervical lesions and malignant tumors. *Am. J. Clin. Pathol.* **143**:344–351.
- Wang, X., Xu, H.R., Li, T., Qu, L., Zhao, Z.D., and Zhang, Z.Y.** (2014). Expression analysis of KAP9.2 and Hoxc13 genes during different cashmere growth stages by qRT-PCR method. *Mol. Biol. Rep.* **41**:5665–5668.
- Wang, Y., Tang, H., DeBarry, J.D., Tan, X., Li, J., Wang, X., Lee, T.H., Jin, H., Marler, B., Guo, H., et al.** (2012). MCScanX: a toolkit for detection and evolutionary analysis of gene synteny and collinearity. *Nucleic Acids Res.* **40**:e49.
- Wei, C., Yang, H., Wang, S., Zhao, J., Liu, C., Gao, L., Xia, E., Lu, Y., Tai, Y., She, G., et al.** (2018). Draft genome sequence of *Camellia sinensis* var. *sinensis* provides insights into the evolution of the tea genome and tea quality. *Proc. Natl. Acad. Sci. USA* **115**:E4151–E4158.
- Werker, E.** (2000). Trichome diversity and development. *Adv. Bot. Res.* **31**:1–35.
- Wheeler, T.J., Clements, J., Eddy, S.R., Hubley, R., Jones, T.A., Jurka, J., Smit, A.F.A., and Finn, R.D.** (2013). Dfam: a database of repetitive DNA based on profile hidden Markov models. *Nucleic Acids Res.* **41**:D70–D82. –D82.
- Wood, T.E., Takebayashi, N., Barker, M.S., Mayrose, I., Greenspoon, P.B., and Rieseberg, L.H.** (2009). The frequency of polyploid

- speciation in vascular plants. Proc. Natl. Acad. Sci. USA **106**:13875–13879.
- Wu, Y.B., Ni, Z.Y., Shi, Q.W., Dong, M., Kiyota, H., Gu, Y.C., and Cong, B.** (2012). Constituents from *Salvia* species and their biological activities. Chem. Rev. **112**:5967–6026.
- Wu, Z.Y.** (1977). Flora of China (Beijing: Science Press), pp. 194–198.
- Xia, E., Tong, W., Hou, Y., An, Y., Chen, L., Wu, Q., Liu, Y., Yu, J., Li, F., Li, R., et al.** (2020). The reference genome of tea plant and resequencing of 81 diverse accessions provide insights into genome evolution and adaptation of tea plants. Mol. Plant **13**:1013–1026.
- Xiang, Y., An, S., Cheng, M., Liu, L., and Xie, Y.** (2018). Changes of soil microbiological properties during grass litter decomposition in Loess Hilly Region, China. Int. J. Environ. Res. Public Health **15**:1797.
- Xie, T., Zheng, J.F., Liu, S., Peng, C., Zhou, Y.M., Yang, Q.Y., and Zhang, H.Y.** (2015). *De novo* plant genome assembly based on chromatin interactions: a case study of *Arabidopsis thaliana*. Mol. Plant **8**:489–492.
- Xu, H., Song, J., Luo, H., Zhang, Y., Li, Q., Zhu, Y., Xu, J., Li, Y., Song, C., Wang, B., et al.** (2016a). Analysis of the genome sequence of the medicinal plant *Salvia miltiorrhiza*. Mol. Plant **9**:949–952.
- Xu, Y., Bi, C., Wu, G., Wei, S., Dai, X., Yin, T., and Ye, N.** (2016b). VGSC: a web-based vector graph toolkit of genome synteny and collinearity. BioMed Res. Int. **2019**:2150291.
- Xu, Z., and Wang, H.** (2007). LTR\_FINDER: an efficient tool for the prediction of full-length LTR retrotransposons. Nucleic Acids Res. **35**:W265–W268.
- Yan, T., Chen, M., Shen, Q., Li, L., Fu, X., Pan, Q., Tang, Y., Shi, P., Lv, Z., Jiang, W., et al.** (2017). HOMEODOMAIN PROTEIN 1 is required for jasmonate-mediated glandular trichome initiation in *Artemisia annua*. New Phytol. **213**:1145–1155.
- Yan, T., Li, L., Xie, L., Chen, M., Shen, Q., Pan, Q., Fu, X., Shi, P., Tang, Y., Huang, H., et al.** (2018). A novel HD-ZIP'/MIXTA complex promotes glandular trichome initiation and cuticle development in *Artemisia annua*. New Phytol. **218**:567–578.
- Yang, Z.** (1997). PAML: a program package for phylogenetic analysis by maximum likelihood. Comput. Appl. Biosci. **13**:555–556.
- Yu, G., Wang, L.G., Han, Y., and He, Q.Y.** (2012). clusterProfiler: an R package for comparing biological themes among gene clusters. OMICS A J. Integr. Biol. **16**:284–287.
- Zhang, X., Yan, F., Tang, Y., Yuan, Y., Deng, W., and Li, Z.** (2015). Auxin response gene SIARF3 plays multiple roles in tomato development and is involved in the formation of epidermal cells and trichomes. Plant Cell Physiol. **56**:2110–2124.
- Zhang, X., Zhang, S., Zhao, Q., Ming, R., and Tang, H.** (2019). Assembly of allele-aware, chromosomal-scale autoploid genomes based on Hi-C data. Nat. Plants **5**:833–845.
- Zhao, Q., Chen, X.Y., and Martin, C.** (2016). *Scutellaria baicalensis*, the golden herb from the garden of Chinese medicinal plants. Sci. Bull. **61**:1391–1398.
- Zhao, Q., Yang, J., Cui, M.Y., Liu, J., Fang, Y., Yan, M., Qiu, W., Shang, H., Xu, Z., Yidiressi, R., et al.** (2019). The reference genome sequence of *Scutellaria baicalensis* provides insights into the evolution of wogonin biosynthesis. Mol. Plant **12**:935–950.
- Zhou, F., and Pichersky, E.** (2020). More is better: the diversity of terpene metabolism in plants. Curr. Opin. Plant Biol. **55**:1–10.
- Zhou, Z., Tan, H., Li, Q., Li, Q., Wang, Y., Bu, Q., Li, Y., Wu, Y., Chen, W., and Zhang, L.** (2020). TRICHOME AND ARTEMISININ REGULATOR 2 positively regulates trichome development and artemisinin biosynthesis in *Artemisia annua*. New Phytol. **228**:932–945.
- Zwaenepoel, A., and Van de Peer, Y.** (2019). wgd-simple command line tools for the analysis of ancient whole-genome duplications. Bioinformatics **35**:2153–2155.

**Supplemental information**

**Chromosome-level assembly and analysis of the *Thymus* genome provide insights into glandular secretory trichome formation and monoterpenoid biosynthesis in thyme**

**Meiyu Sun, Yanan Zhang, Li Zhu, Ningning Liu, Hongtong Bai, Guofeng Sun, Jinzheng Zhang, and Lei Shi**

---

**Chromosome-level assembly and analysis of the *Thymus* genome provide insights on glandular secretory trichome formation and monoterpenoid biosynthesis in thyme**

Meiyu Sun<sup>1#</sup>, Yanan Zhang<sup>1,2#</sup>, Li Zhu<sup>1,2</sup>, Ningning Liu<sup>1,2</sup>, Hongtong Bai<sup>1</sup>, Guofeng Sun<sup>3</sup>, Jinzheng Zhang<sup>1\*</sup> and Lei Shi<sup>1\*</sup>

<sup>1</sup> Key Laboratory of Plant Resources and Beijing Botanical Garden, Institute of Botany, Chinese Academy of Sciences, Beijing 100093, China.

<sup>2</sup> University of Chinese Academy of Sciences, Beijing 100049, China.

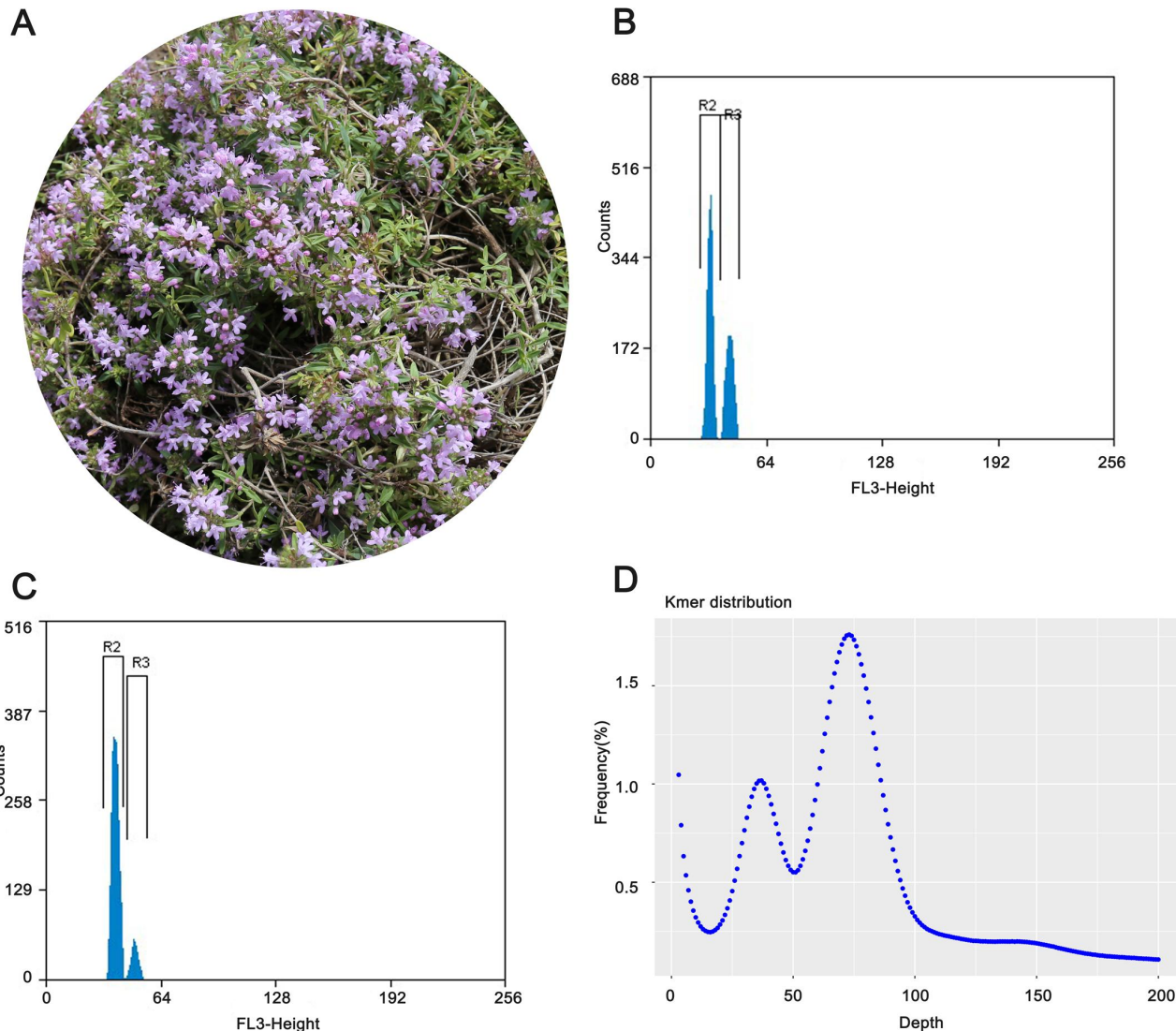
<sup>3</sup> Beijing Botanical Garden, Institute of Botany, Chinese Academy of Sciences, Beijing 100093, China.

# These authors contributed equally to this work.

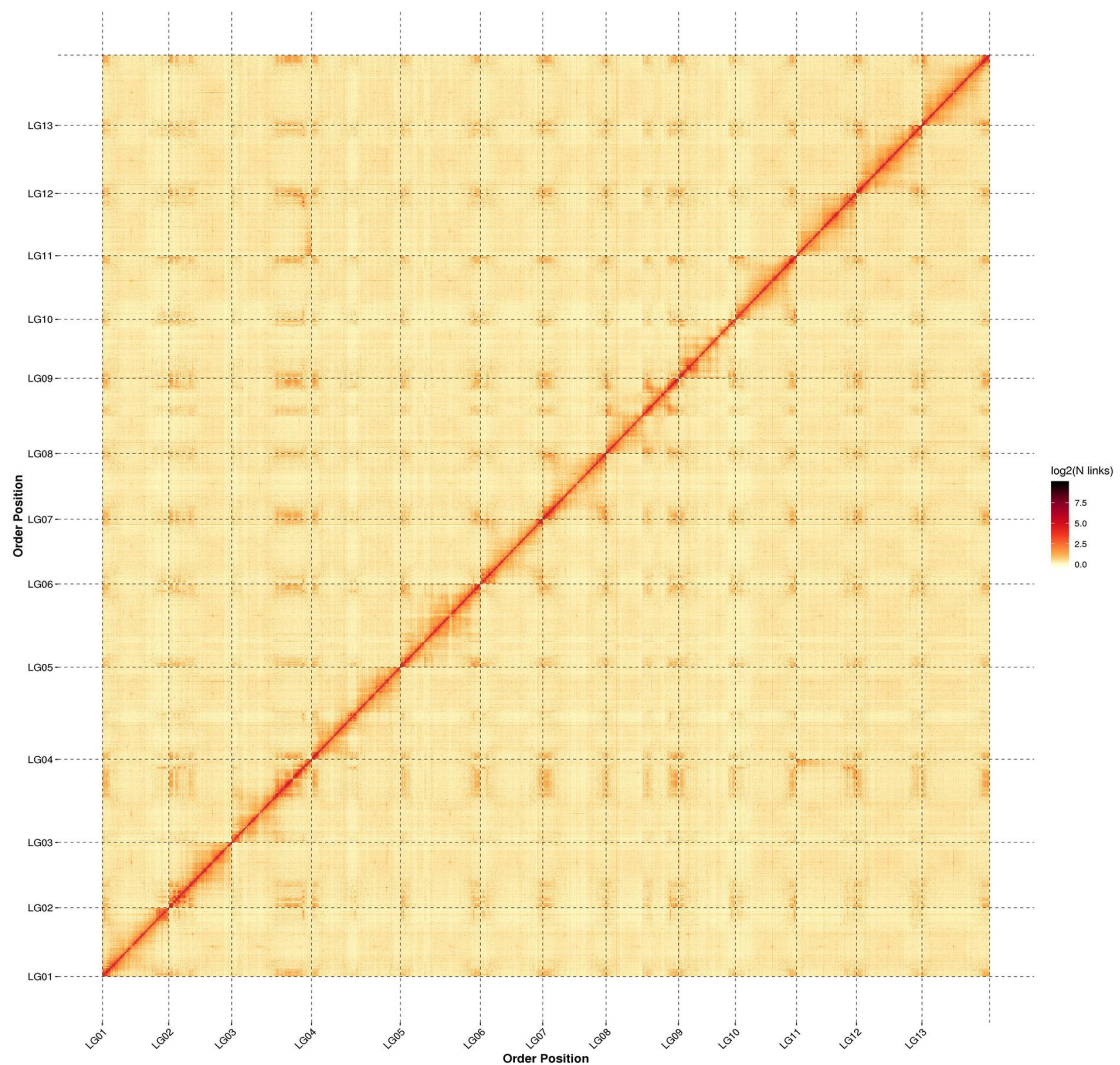
\*Correspondence: Lei Shi (shilei\_67@126.com), Jinzheng Zhang (caohua@ibcas.ac.cn)

---

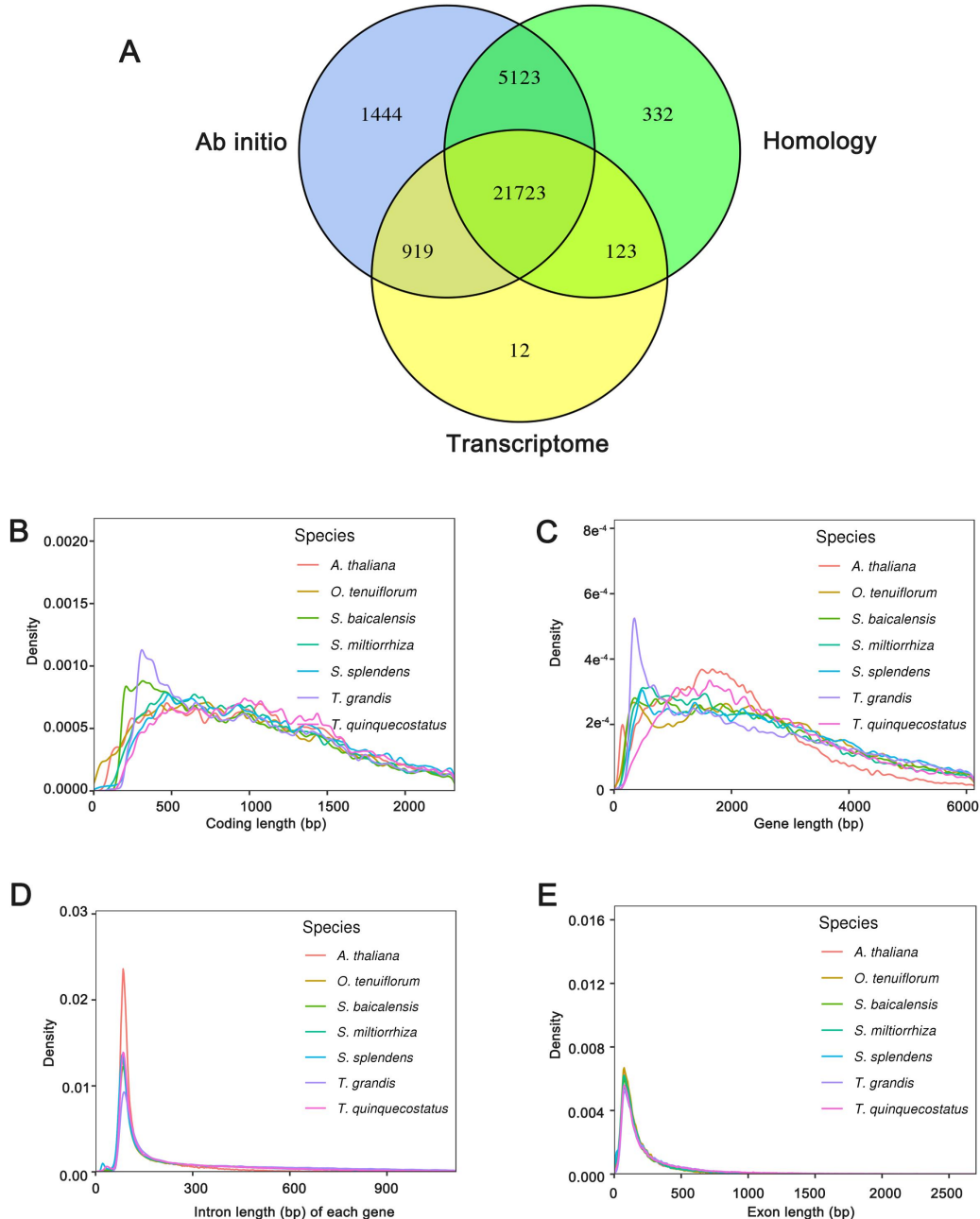
## Supplementary Figures



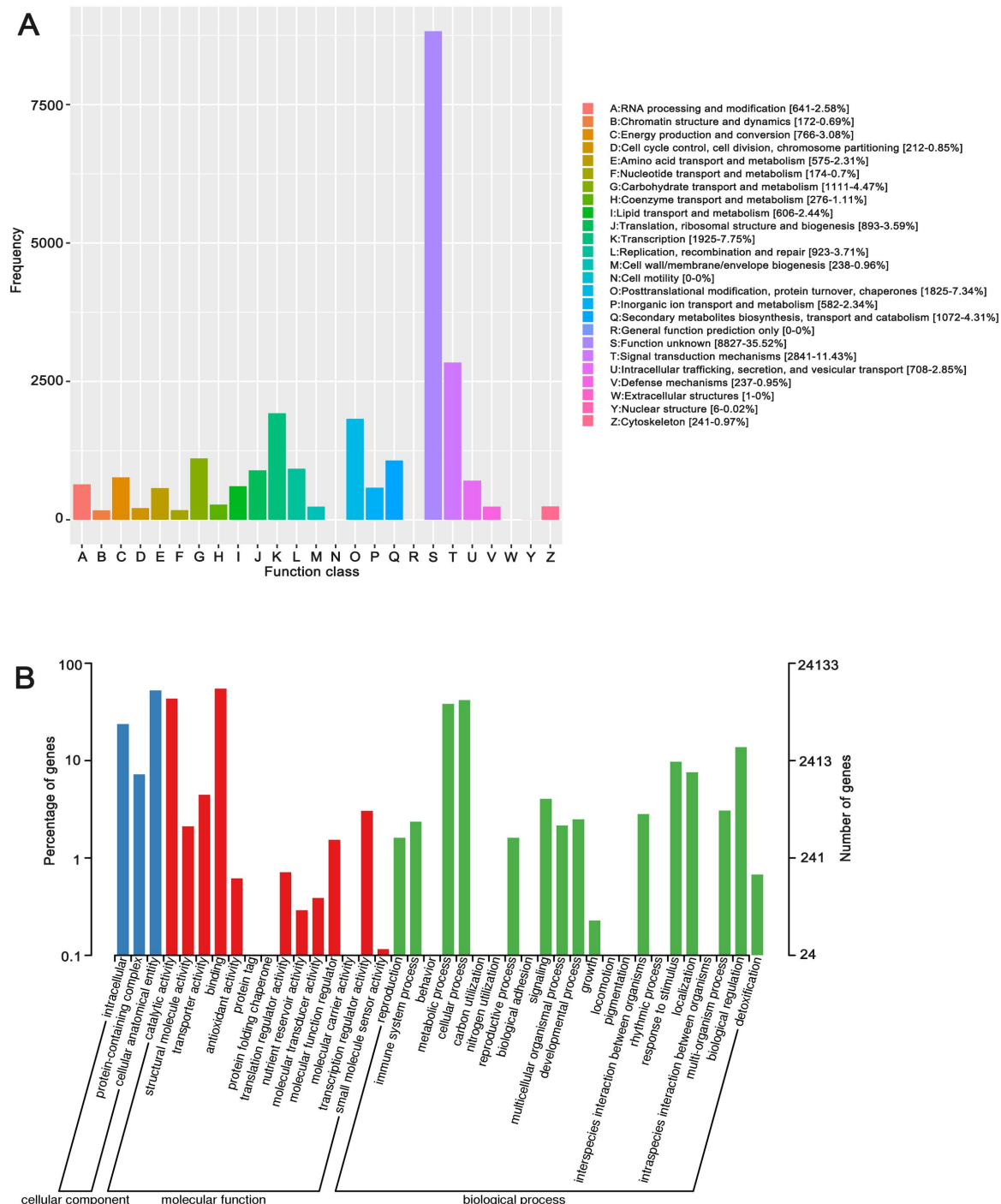
**Supplemental Figure 1. Image exhibition, flow cytometry estimation and k-mer distribution analysis of *T. quinquecostatus*.** **(A)** The flower image of *T. quinquecostatus* (CNT39, NCBI: TaxID 228974). **(B)** The genome size of *T. quinquecostatus* was estimated using *Oryza sativa* ssp. *indica* (93-11, 393.5 Mb). **(C)** The genome size of *T. quinquecostatus* was estimated using *Sorghum bicolor* L. (Tx430, 732.2Mb). **(D)** The genome size of *T. quinquecostatus* was estimated based on k-mer counting.



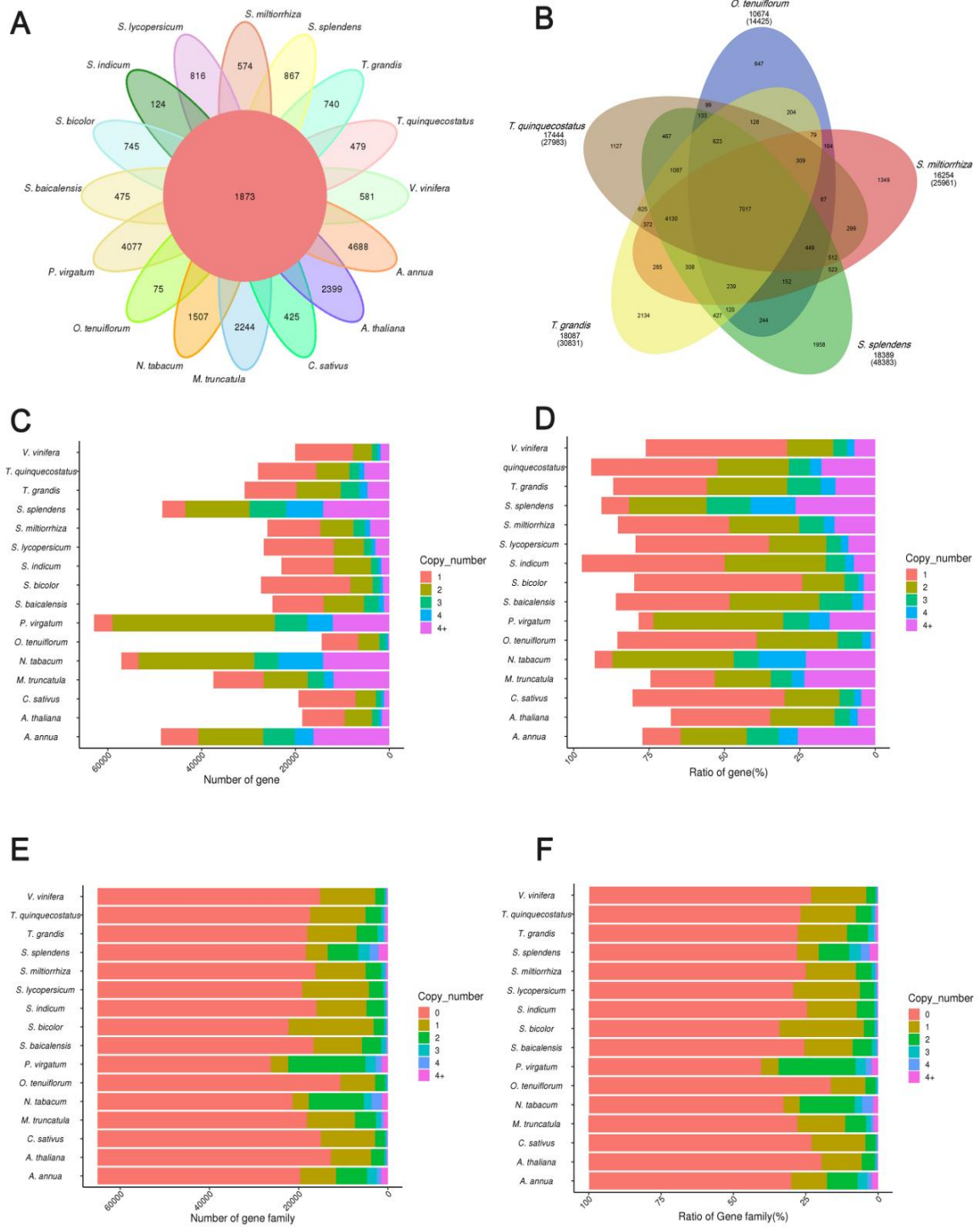
**Supplemental Figure 2. The genome-wide Hi-C heat map of chromosome interactions in *T. quinquecostatus*.** The intensity of pixels represents the count of Hi-C links between 100 kb windows on 13 pseudochromosomes on a logarithmic scale.



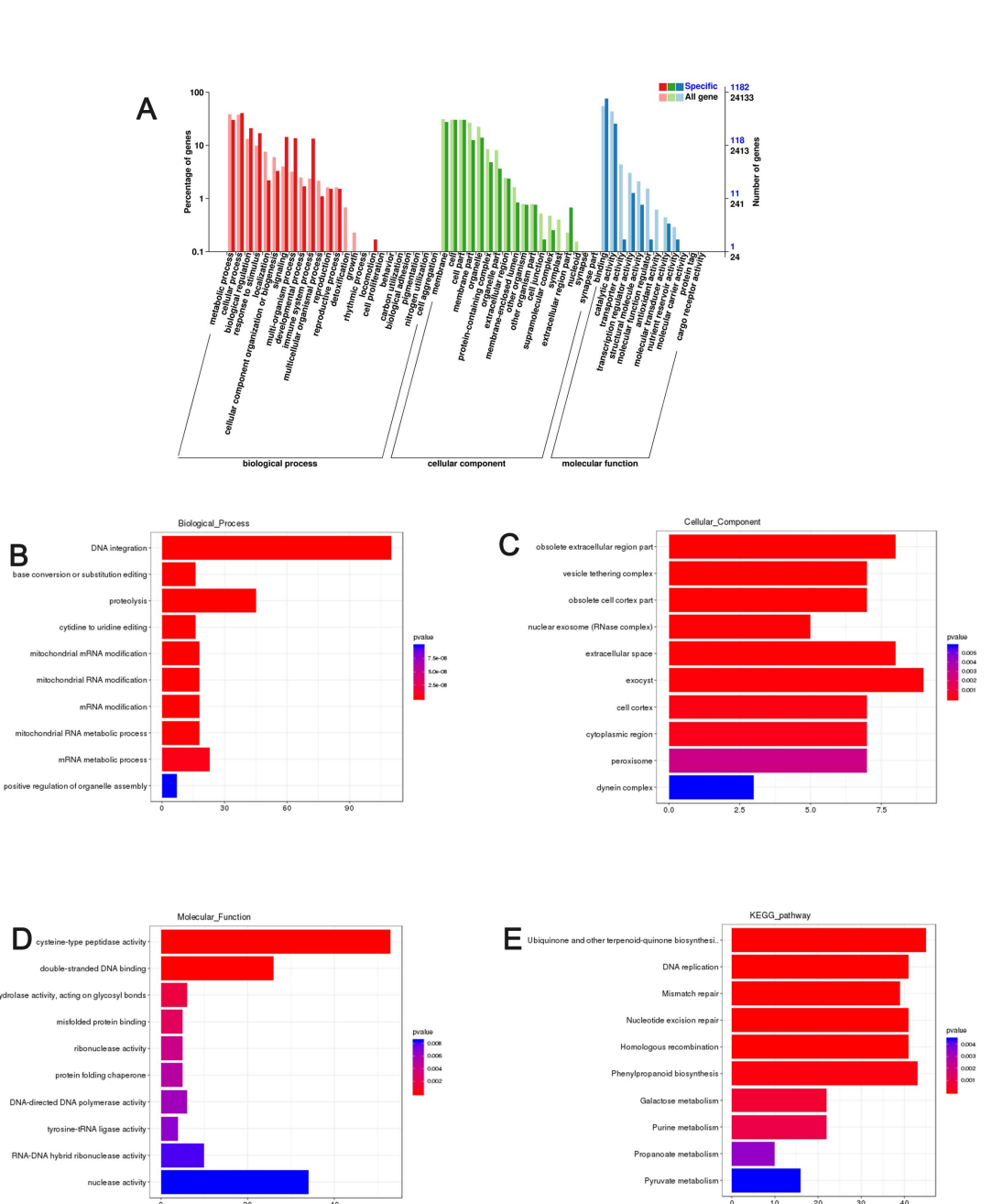
**Supplemental Figure 3. Predicted protein-coding genes were predicted in *T. quinquecostatus*. (A)** Venn diagram showing protein-coding genes were predicted on the basis of 3 different strategies. **(B)** The coding length of protein-coding genes in *T. quinquecostatus* and related species. **(C)** The gene length of protein-coding genes in *T. quinquecostatus* and related species. **(D)** The intron length of protein-coding genes in *T. quinquecostatus* and related species. **(E)** The exon length of protein-coding genes in *T. quinquecostatus* and related species.



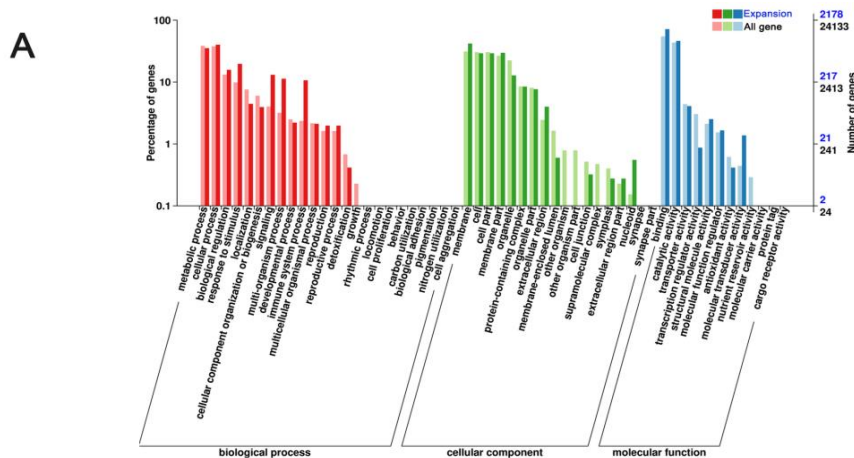
**Supplemental Figure 4. Enrichment analysis of protein-coding genes in *T. quinquecostatus*. (A)** eggNOG enrichment analysis of protein-coding genes in *T. quinquecostatus*. **(B)** GO enrichment analysis of protein-coding genes in *T. quinquecostatus*.



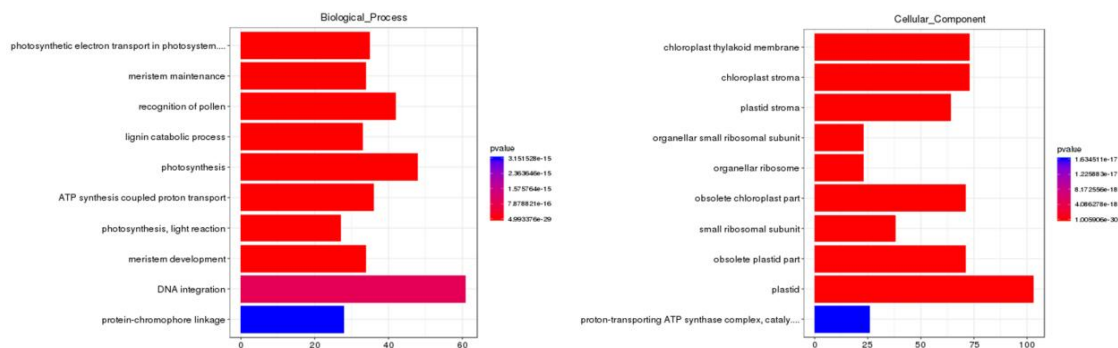
**Supplemental Figure 5. Cluster analysis of gene and gene families in *T. quinquecostatus* and other 15 related species.** **(A)** Petal diagram of gene families cluster in 16 species. **(B)** Venn diagram of gene families cluster in 5 Labiaceae species. **(C)** The number of copies distribution of all genes in 16 species. **(D)** The ratio of copies distribution of all genes in 16 species. **(E)** The number of copies distribution of all gene families in 16 species. **(F)** The ratio of copies distribution of all gene families in 16 species.



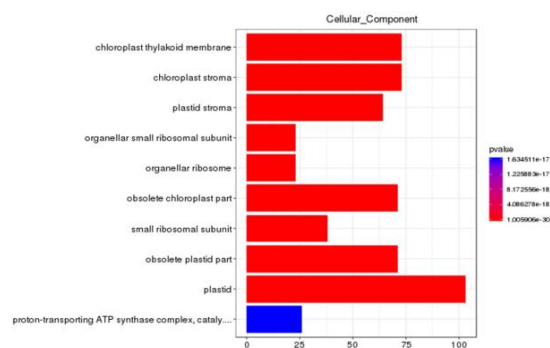
**Supplemental Figure 6. Cluster analysis of specific genes in *T. quinquecostatus*. (A)** GO enrichment analysis of specific genes in *T. quinquecostatus*. **(B)** Biological process enrichment analysis of specific genes in *T. quinquecostatus*. **(C)** Cellular component enrichment analysis of specific genes in *T. quinquecostatus*. **(D)** Molecular function enrichment analysis of specific genes in *T. quinquecostatus*. **(E)** KEGG enrichment analysis of specific genes in *T. quinquecostatus*.



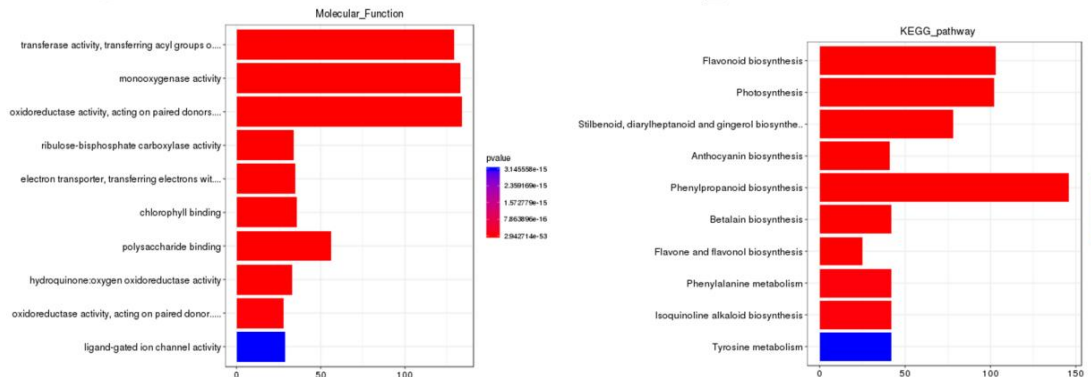
**B**



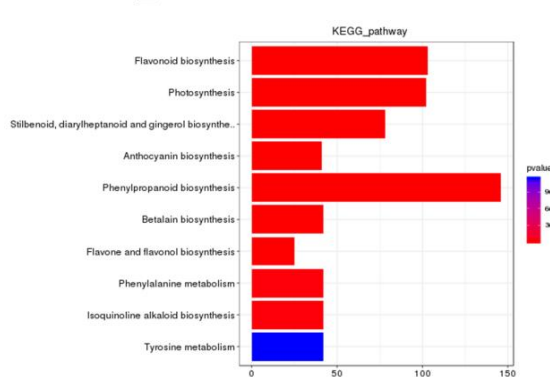
**C**



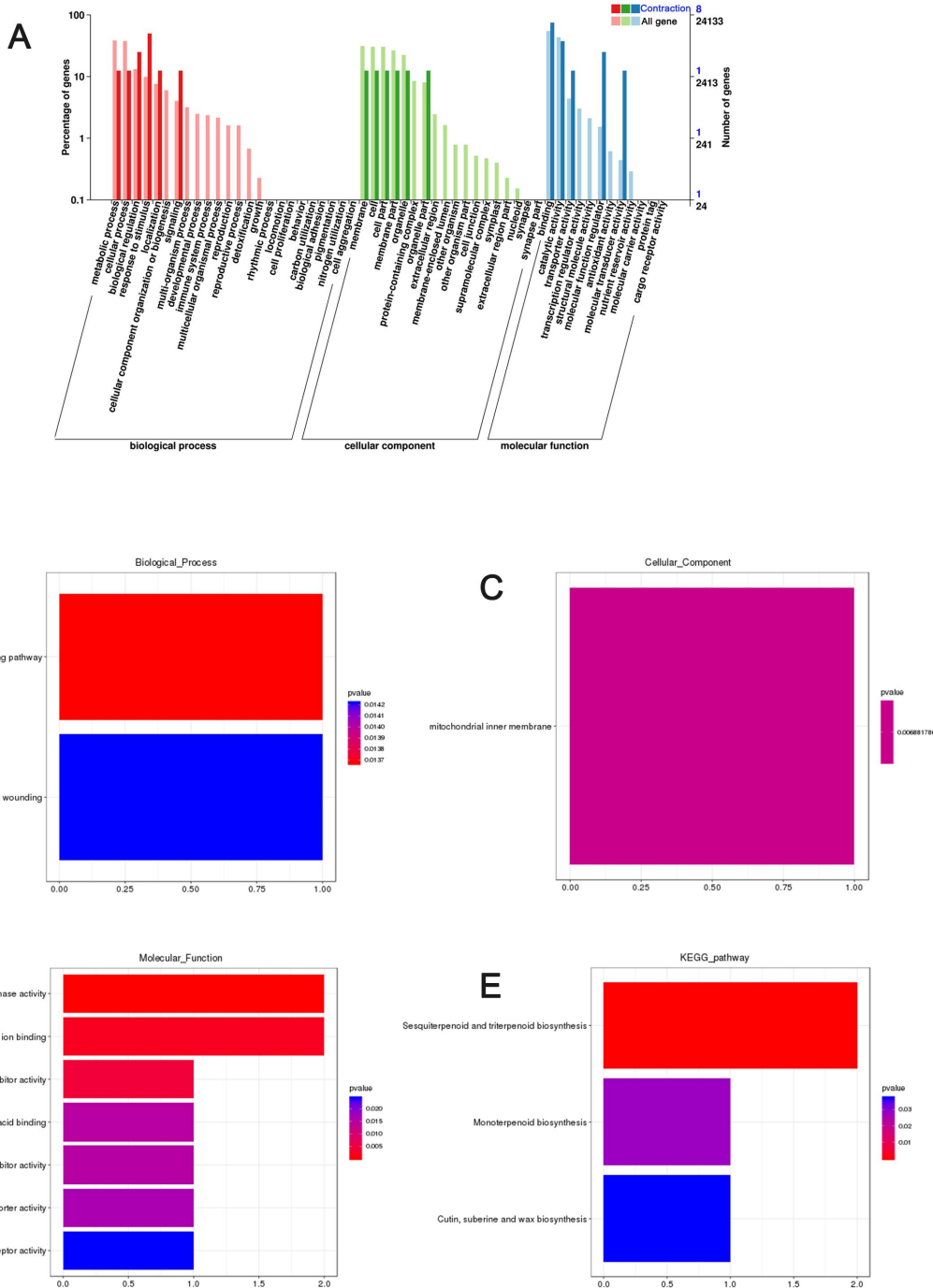
**D**



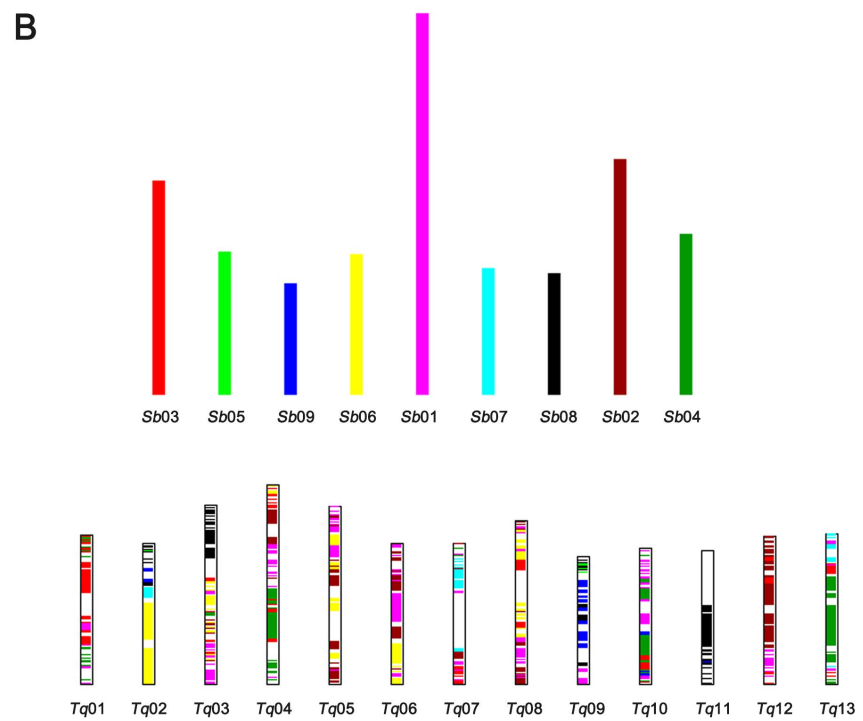
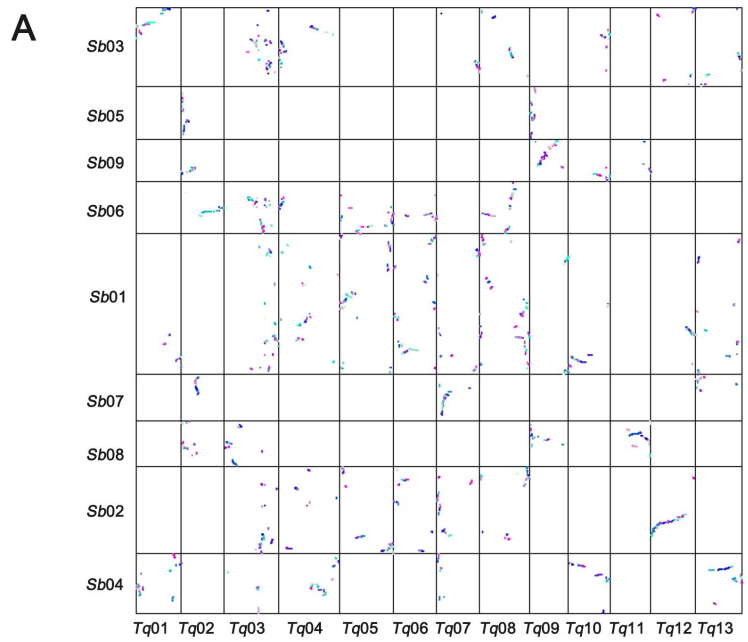
**E**



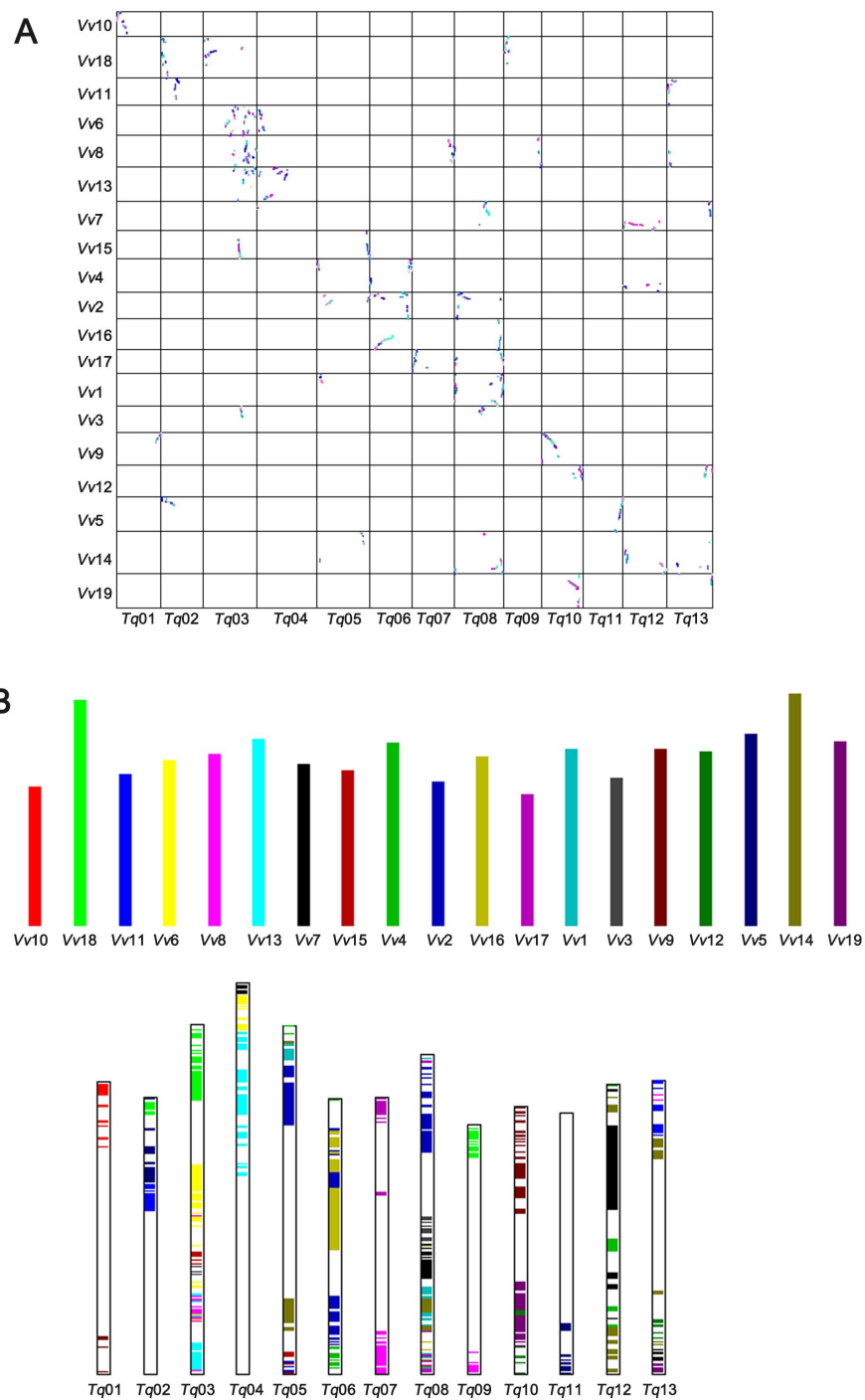
**Supplemental Figure 7. Cluster analysis of expansion genes in *T. quinquecostatus*. (A)** GO enrichment analysis of expansion genes in *T. quinquecostatus*. **(B)** Biological process enrichment analysis of expansion genes in *T. quinquecostatus*. **(C)** Cellular component enrichment analysis of expansion genes in *T. quinquecostatus*. **(D)** Molecular function enrichment analysis of expansion genes in *T. quinquecostatus*. **(E)** KEGG enrichment analysis of expansion genes in *T. quinquecostatus*.



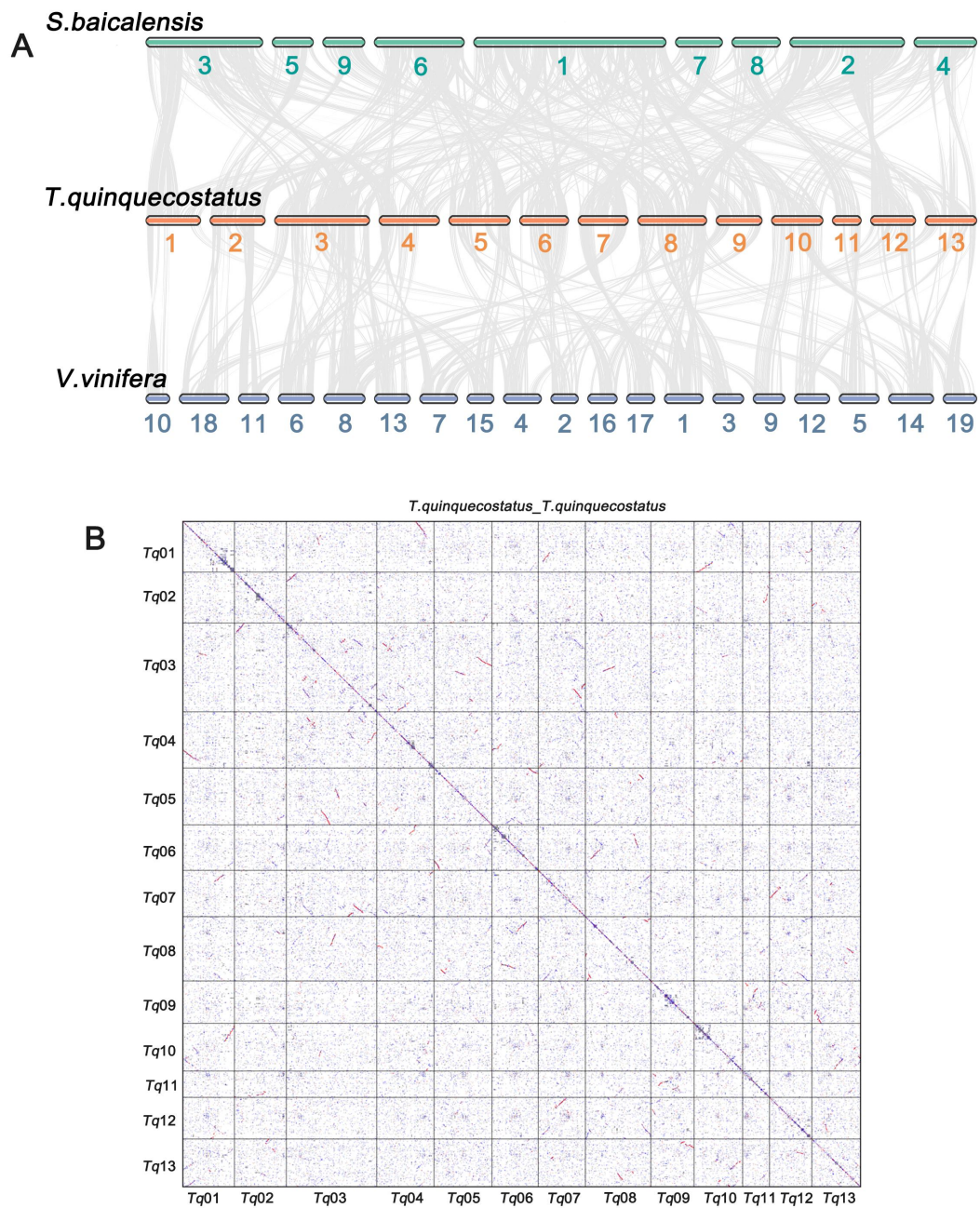
**Supplemental Figure 8. Cluster analysis of contraction genes in *T. quinquecostatus*. (A)** GO enrichment analysis of contraction genes in *T. quinquecostatus*. **(B)** Biological process enrichment analysis of contraction genes in *T. quinquecostatus*. **(C)** Cellular component enrichment analysis of contraction genes in *T. quinquecostatus*. **(D)** Molecular function enrichment analysis of contraction genes in *T. quinquecostatus*. **(E)** KEGG enrichment analysis of contraction genes in *T. quinquecostatus*.



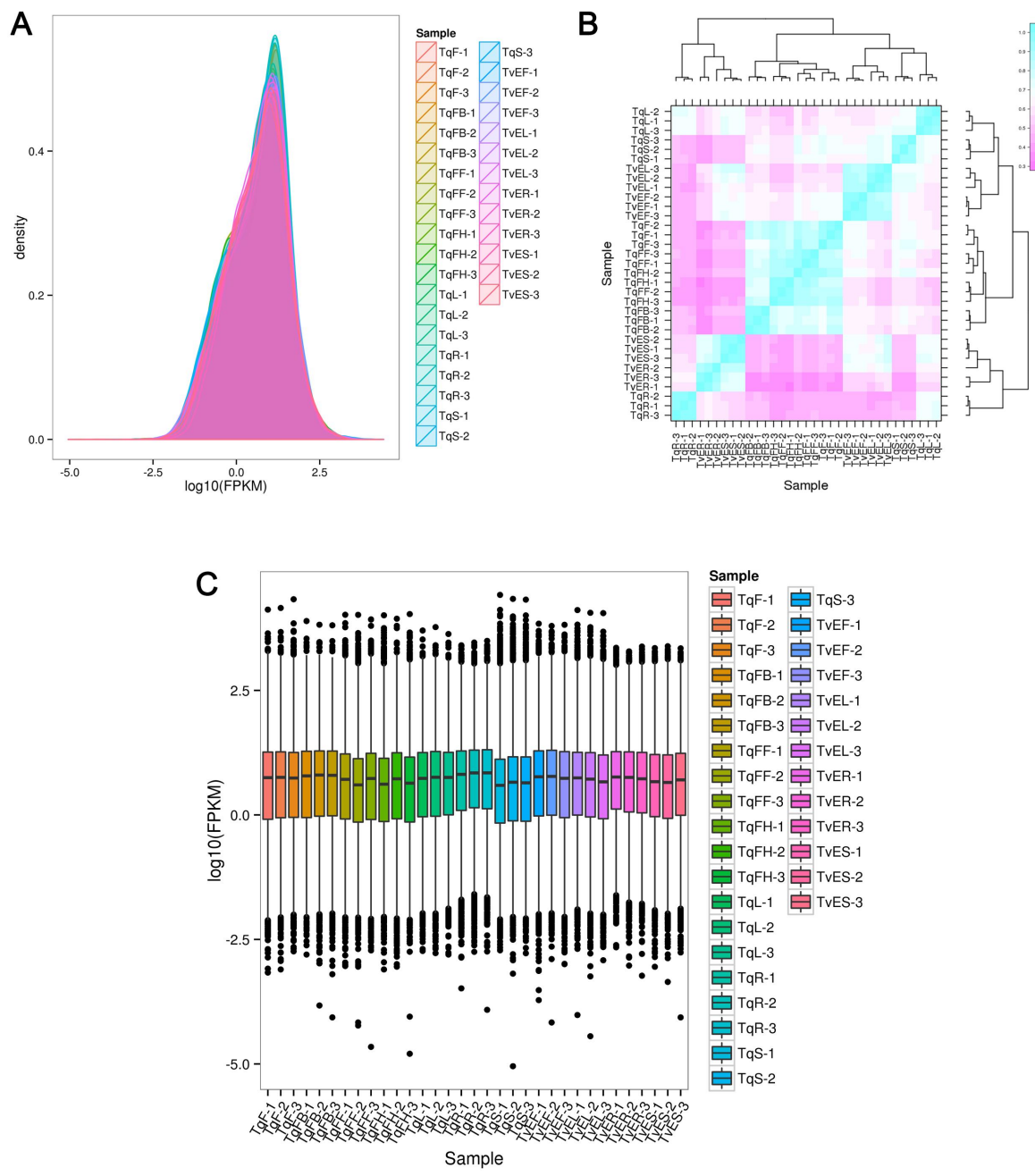
**Supplemental Figure 9. Visualization of collinear blocks between *T. quinquecostatus* and *S. baicalensis*.** **(A)** The dot graphs of synteny blocks between *T. quinquecostatus* and *S. baicalensis*. Dots closest to the diagonal line represent collinearity between the two genomes with < 10 Kb fragments filtered out. **(B)** The bar graphs of synteny blocks between *T. quinquecostatus* and *S. baicalensis*.



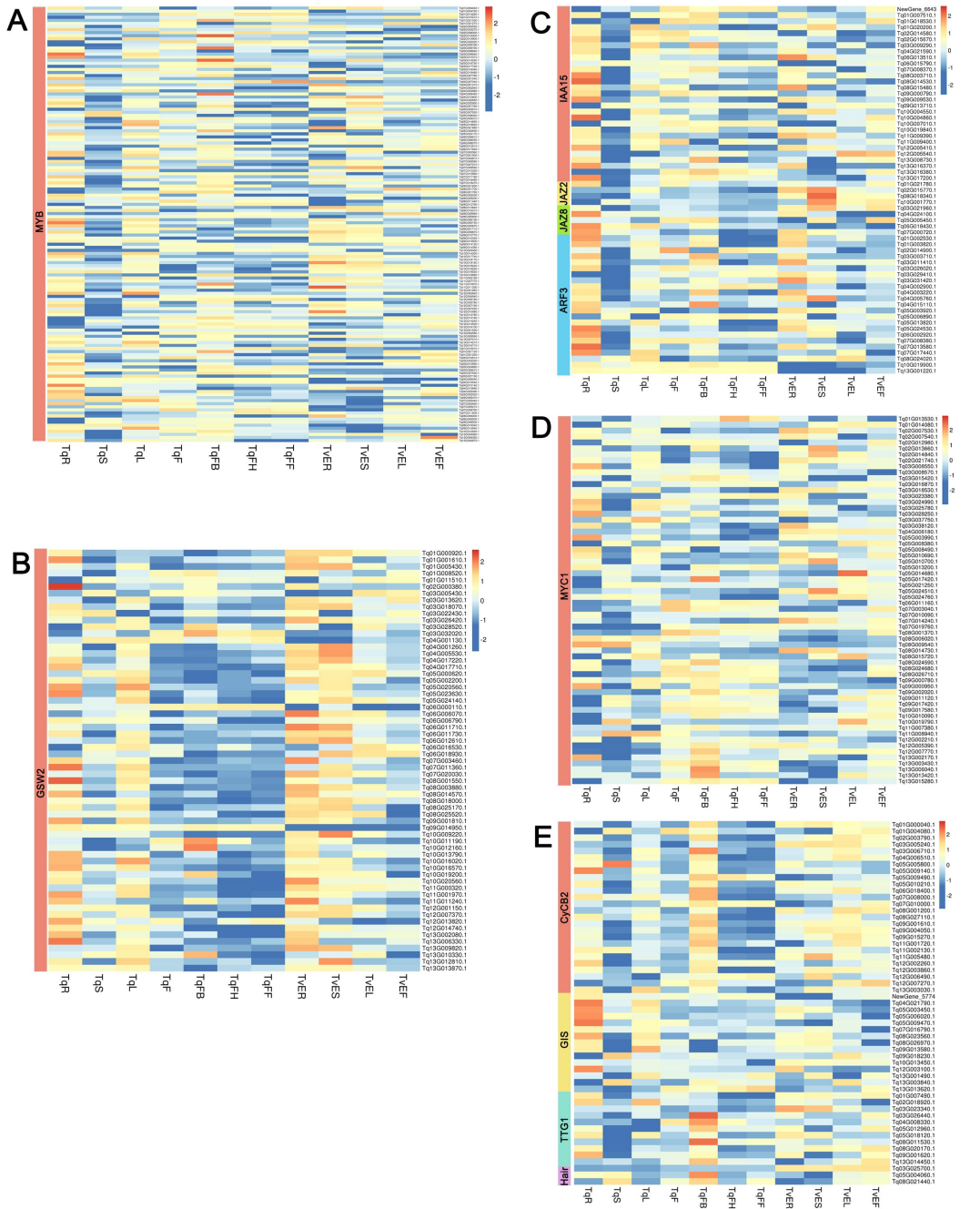
**Supplemental Figure 10. Visualization of collinear blocks between *T. quinquecostatus* and *V. vinifera*.** (A) The dot graphs of synteny blocks between *T. quinquecostatus* and *V. vinifera*. Dots closest to the diagonal line represent collinearity between the two genomes with < 10 Kb fragments filtered out. (B) The bar graphs of synteny blocks between *T. quinquecostatus* and *V. vinifera*.



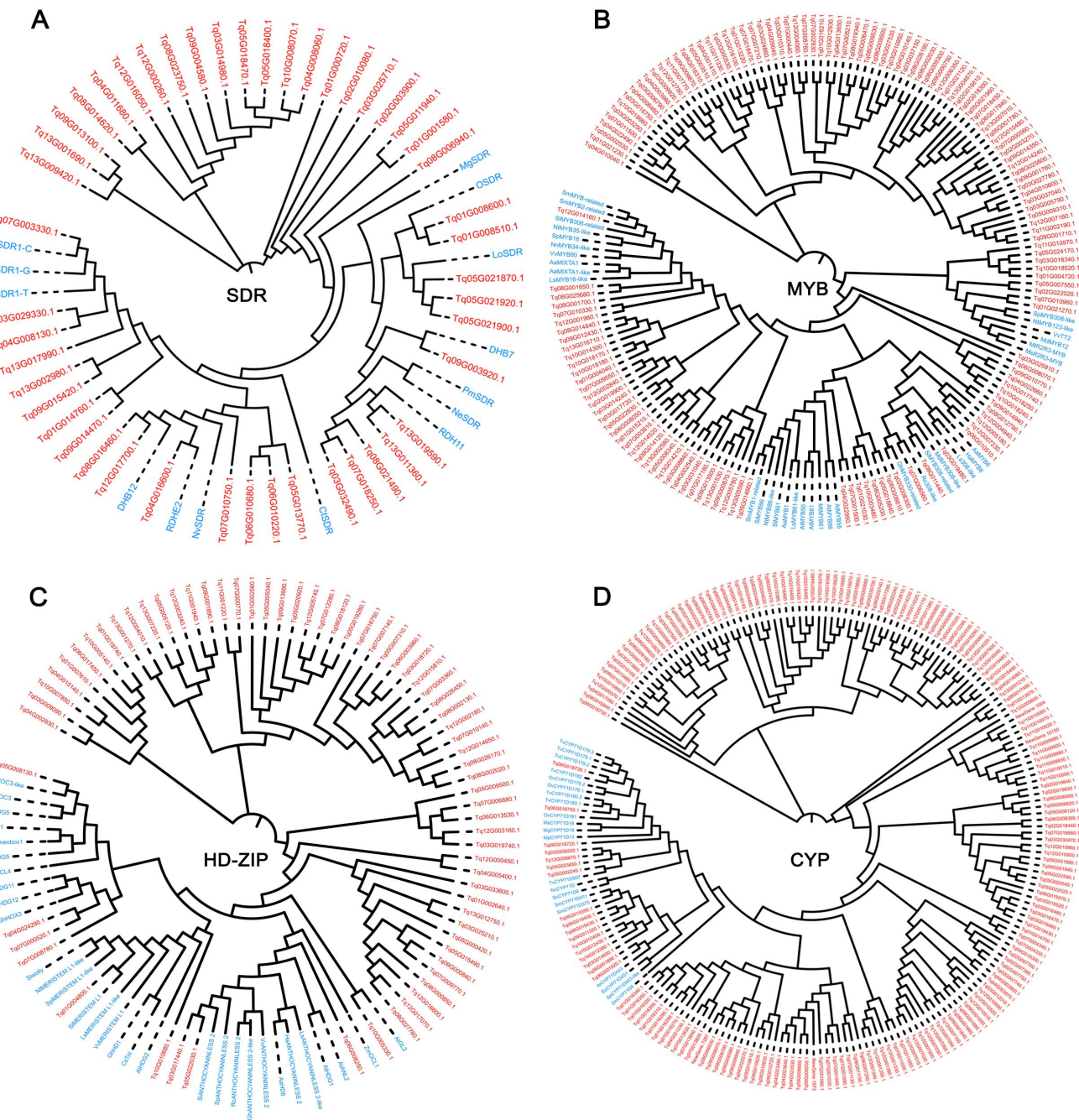
**Supplemental Figure 11. Visualization of collinear blocks between *T. quinquecostatus*, *S. baicalensis* and *V. vinifera*.** (A) Comparison of the karyotype between *T. quinquecostatus*, *S. baicalensis* and *V. vinifera*. (B) The dot graphs of synteny blocks of *T. quinquecostatus* genome. The gene set of *T. quinquecostatus* was self-aligned using blast program. The alignment result was then fed to MCScanX package for synteny blocks identification. The X- and Y-axis represent the 13 chromosomes of *T. quinquecostatus*, respectively.



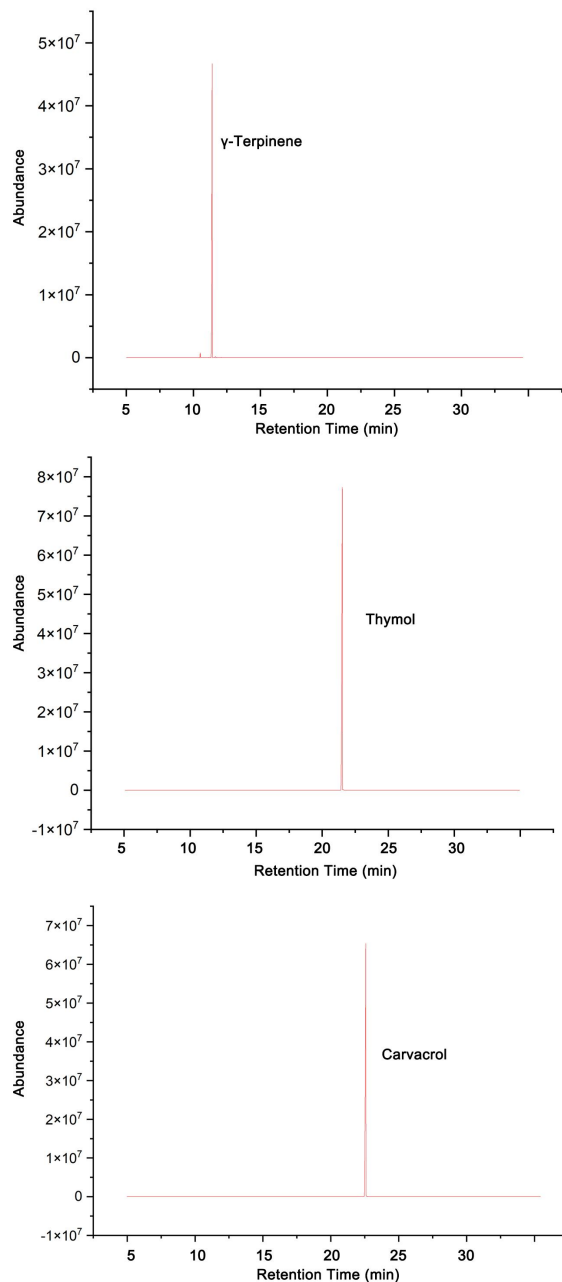
**Supplemental Figure 12. Results of thyme transcriptome sequencing. (A)** Density of FPKM in 33 samples. **(B)** Heatmap of 33 samples. **(C)** Box of FPKM in 33 samples.



**Supplemental Figure 13. Expression heatmap of other key DEGs involved in glandular secretory trichomes (GSTs) formation mechanism.** (A) Expression heatmap of MYB-encoding genes in GSTs formation mechanism. (B) Expression heatmap of *GSW2s* in GSTs formation mechanism. (C) Expression heatmap of hormone-related genes in GSTs formation mechanism. (D) Expression heatmap of *MYC1s* in GSTs formation mechanism. (E) Expression heatmap of *CyCB2s*, *GIs*, *TTG1s*, and *Hairs* in GSTs formation mechanism. TqS, *T. quinquecostatus* stem; TqL, *T. quinquecostatus* leaf; TqF, *T. quinquecostatus* flower; TqFB, *T. quinquecostatus* flower bud stage; TqFH, *T. quinquecostatus* flower half-bloom stage; TqFF, *T. quinquecostatus* flower full-bloom stage; TvER, *T. vulgaris* 'Elisbeth' root; TvES, *T. vulgaris* 'Elisbeth' stem; TvEL, *T. vulgaris* 'Elisbeth' leaf; TvEF, *T. vulgaris* 'Elisbeth' flower. The bar at the right top marked the normalized FPKM values for both in *T. quinquecostatus* and *T. vulgaris* 'Elisbeth' (red denoted high expression and blue indicated low expression, and expression data were Z-score standardized to -3 to 3 per gene.). All of expression genes showing minimum two-fold changes at  $p < 0.05$  (Student's two tailed t-test).

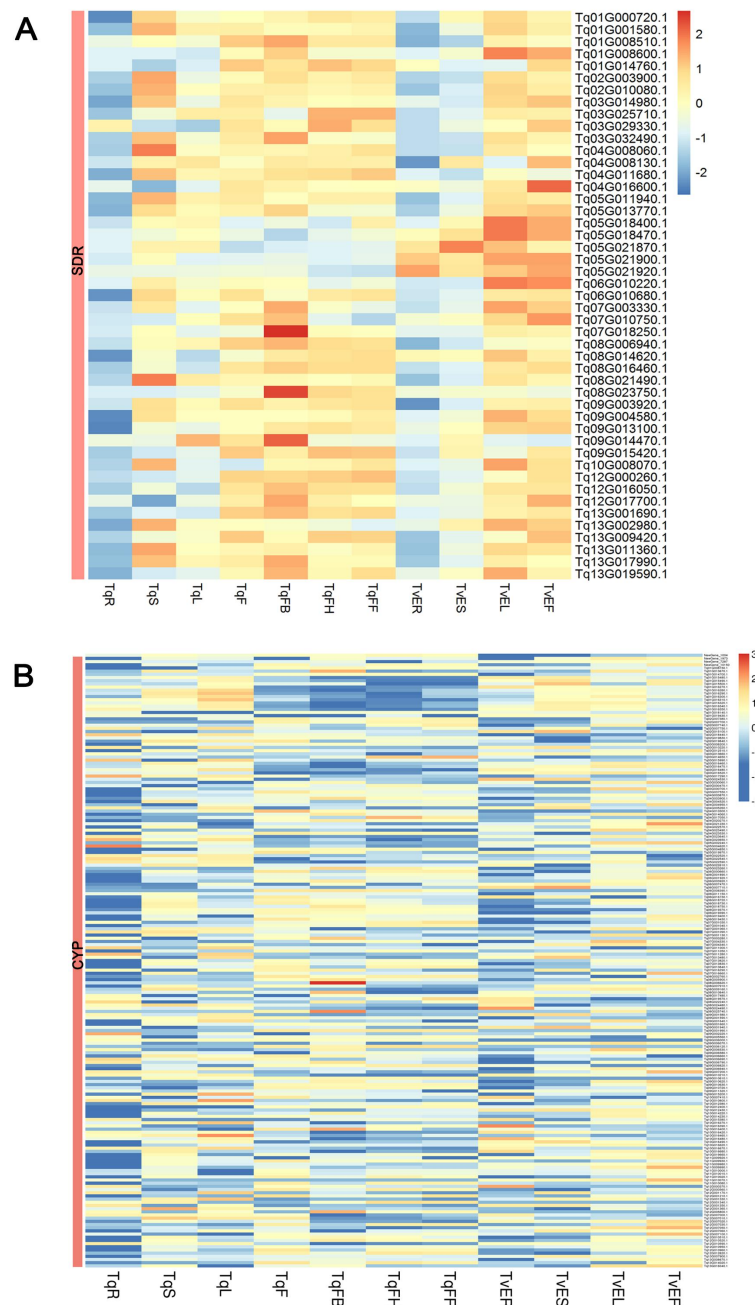


**Supplemental Figure 14. Phylogenetic analysis of SDR-, MYB-, HD-ZIP-, and CYP-encoding genes between the *T. quinquecostatus* and related species.** **(A)** SDR-encoding genes phylogenetic analysis in *T. quinquecostatus* and other related species. **(B)** MYB-encoding genes phylogenetic analysis in *T. quinquecostatus* and other related species. **(C)** HD-ZIP-encoding genes phylogenetic analysis in *T. quinquecostatus* and other related species. **(D)** CYP-encoding genes phylogenetic analysis in *T. quinquecostatus* and other related species.

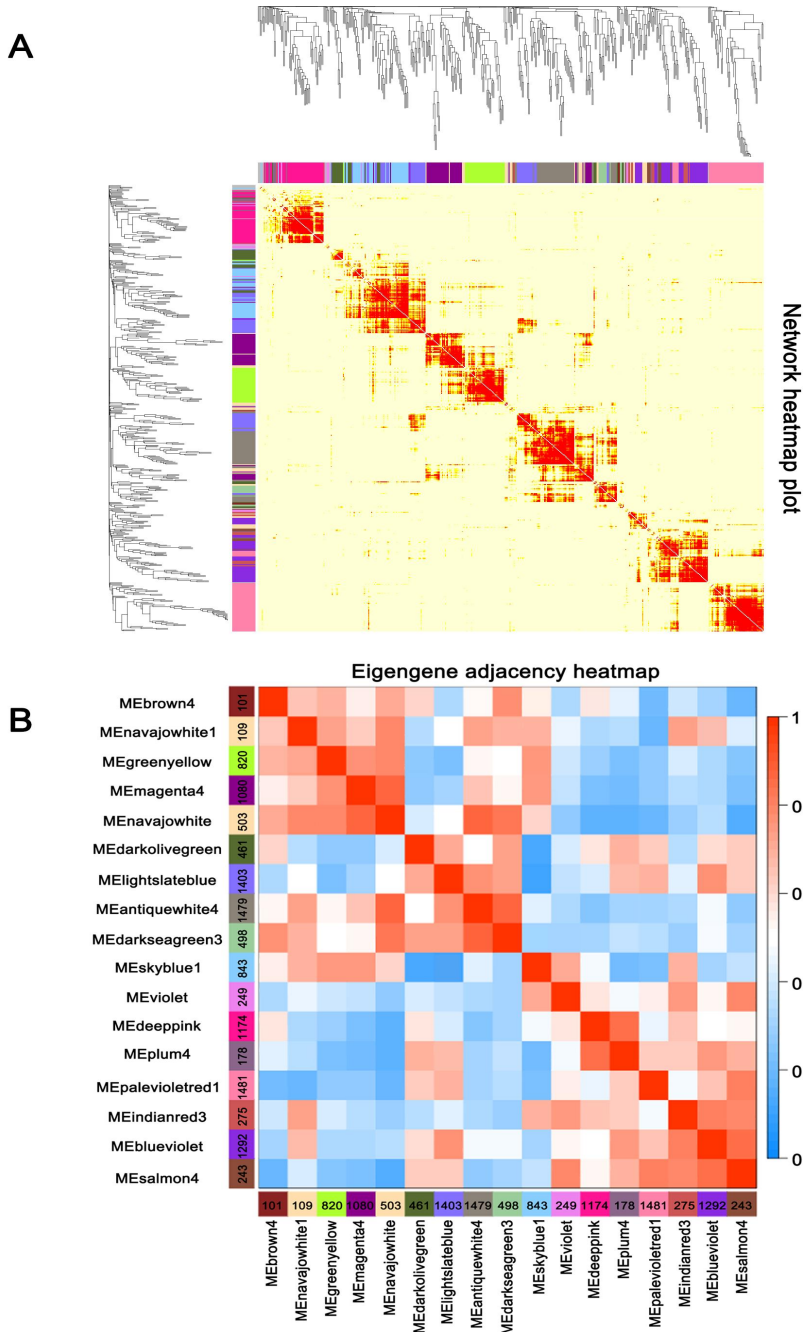


**Supplemental Figure 15. Chromatogram of  $\gamma$ -terpinene, thymol, and carvacrol chemical standards.**

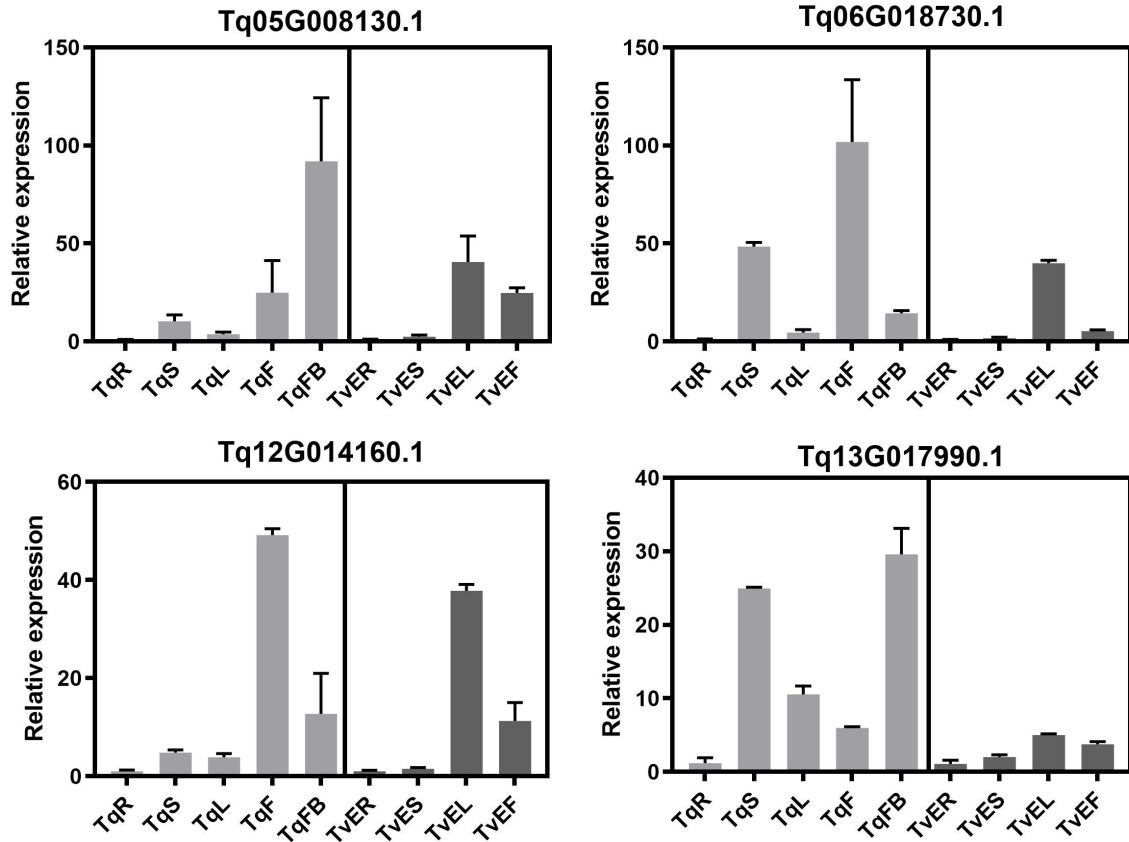
The X-axis represents the retention time of the peak outflow, and the Y-axis represents the response value of the chromatographic peak.



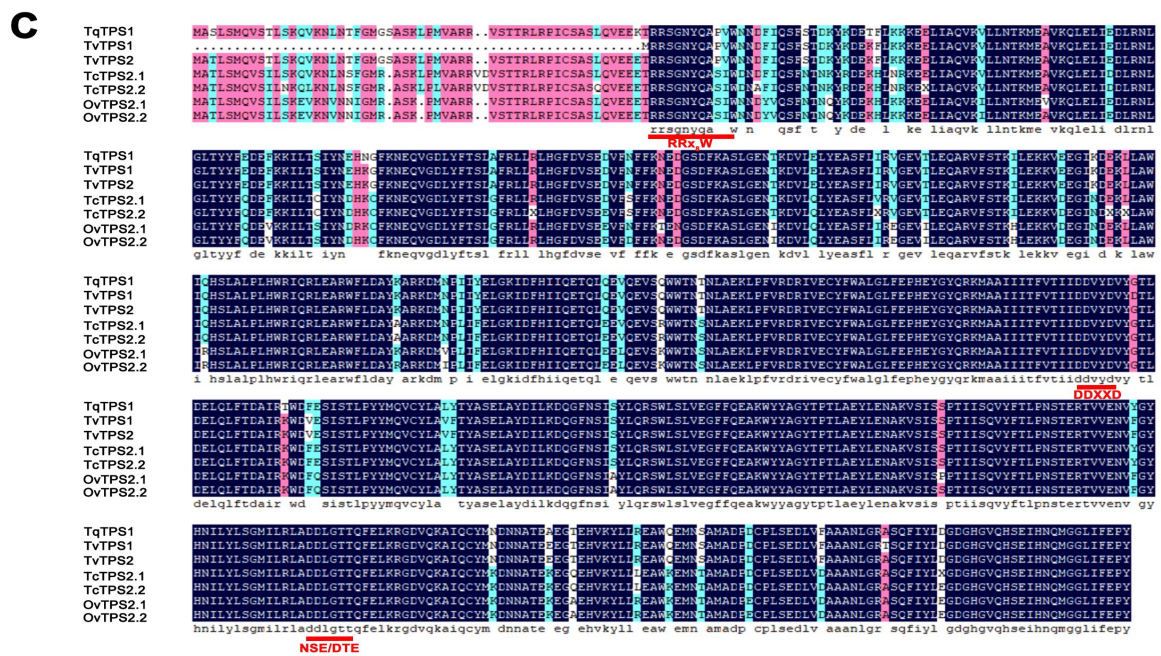
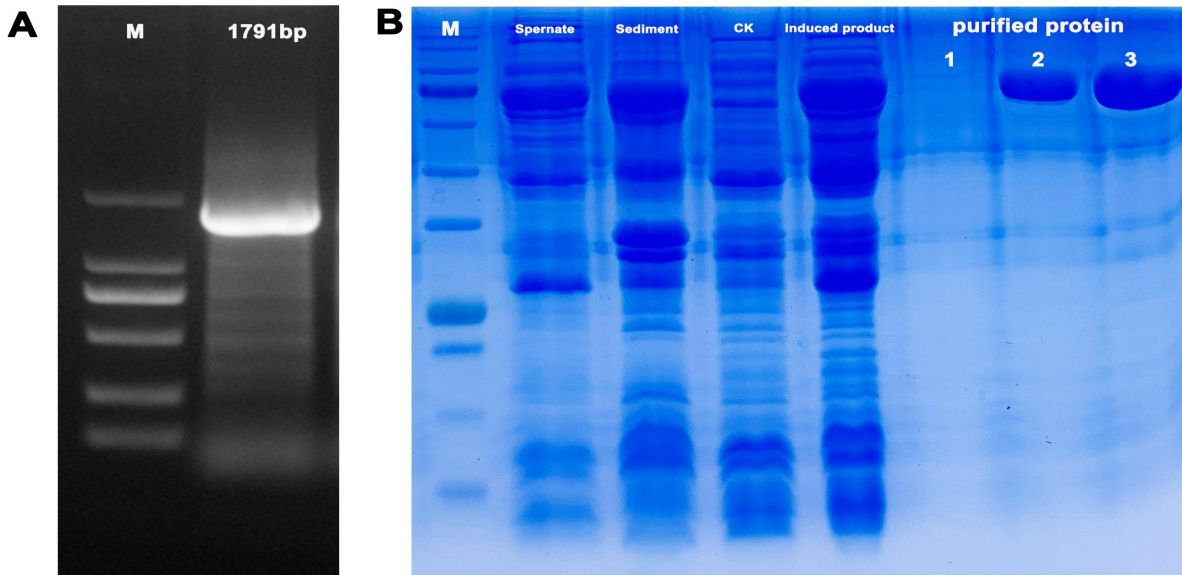
**Supplemental Figure 16. Expression heatmap of SDR- and CYP-encoding genes involved in monoterpenoids biosynthesis.** (A) Heatmap of SDR-encoding genes. (B) Heatmap of CYP-encoding genes. TqR, *T. quinquecostatus* root; TqS, *T. quinquecostatus* stem; TqL, *T. quinquecostatus* leaf; TqF, *T. quinquecostatus* flower; TqFB, *T. quinquecostatus* flower bud stage; TqFH, *T. quinquecostatus* flower half-bloom stage; TqFF, *T. quinquecostatus* flower full-bloom stage; TvER, *T. vulgaris* 'Elsbeth' root; TvES, *T. vulgaris* 'Elsbeth' stem; TvEL, *T. vulgaris* 'Elsbeth' leaf; TvEF, *T. vulgaris* 'Elsbeth' flower. The bar at the right top marked the normalized FPKM values for both in *T. quinquecostatus* and *T. vulgaris* 'Elsbeth' (red denoted high expression and blue indicated low expression, and expression data were Z-score standardized to -3 to 3 per gene.). All of expression genes showing minimum two-fold changes at  $p < 0.05$  (Student's two tailed t-test).



**Supplemental Figure 17. Identification of co-expression network modules in thymes.** **(A)** Network heat map plot. Branches in the hierarchical clustering dendrograms correspond to modules. Color-coded module membership is indicated by the colored bars below and to the right of the dendrograms. In the heat map, high co-expression interconnectedness is indicated by progressively more saturated yellow and red colors. Modules correspond to blocks of highly interconnected genes. Genes with high intramodular connectivity are located at the tip of the module branches because they display the highest interconnectedness with the rest of the genes in the module. **(B)** Module eigengene adjacency heat map. The heat map shows the relatedness of the 17 co-expression modules identified in WGCNA, with red indicating highly related and blue indicating not related.



**Supplemental Figure 18. Quantitative real-time PCR analysis of the *Tq05G008130.1* (*HD-ZIP*), *Tq06G018730.1* (*CYP*), *Tq12G014160.1* (*MYB*), and *Tq13G017990.1* (*SDR*) transcript levels in different tissues of *T. quinquecostatus* and *T. vulgaris* 'Elisbeth', respectively. Amplification of the 18S rRNA gene was used as an internal control. Bars represent the mean and SD of values obtained from three biological replicates.**



**Supplemental Figure 19. Cloning and *in vitro* gene expression in vitro of CDS in *TqTPS1* and amino acid sequence alignment of other TPS proteins. (A) PCR product of CDS in *TqTPS1*. (B) Overexpression of *TqTPS1* analyzed by SDS-PAGE. (C) Amino acid sequence alignment of TPS proteins from *T. quinquecostatus*, *T. caespititus*, *T. vulgaris*, and *Origanum vulgare*. The conserved motifs (RRX<sub>8</sub>W, DDXD and NSE/DTE) are highlighted with red lines.**